Unsaturated Zone Modeling for the Clive PA

28 May 2011

Prepared by

Neptune and Company, Inc.

and

Michael B. Gross

This page is intentionally blank, aside from this statement.

CONTENTS

FIGURES

TABLES

1.0 Summary of Parameter Values

A summary of parameter values used in the Clive DU PA Model is provided in Table 1. For distributions, the following notation is used:

- N(μ, σ, [*min*, *max*]) represents a normal distribution with mean μ and standard deviation σ, and optional truncation at the specified *min*imum and *max*imum,
- LN(*GM*, *GSD*, [*min*, *max*]) represents a log-normal distribution with geometric mean GM and geometric standard deviation GSD, and optional *min* and *max*,
- U(*min*, *max*) represents a uniform distribution with lower bound *min* and upper bound *max*,
- Beta(μ, σ, *min*, *max*) represents a generalized beta distribution with mean μ, standard deviation σ, minimum *min*, and maximum *max*,
- Gamma(μ, σ) represents a gamma distribution with mean μ and standard deviation σ, and
- TRI(*min*, *m*, *max*) represents a triangular distribution with lower bound *min*, mode *m*, and upper bound *max*.

Note that a number of these distributions are truncated at a minimum value of 0 and a maximum of Large, an arbitrarily large value defined in the GoldSim model. The truncation at the low end is a matter of physical limits (e.g. precipitation cannot be negative), and in GoldSim's distribution definitions, if truncations are made, they must be made at both ends, so the very large value is chosen for the upper end.

Table 1: Summary of Parameter Values and Distributions

Parameter	Distribution [*Comments*]	Units	Internal Reference
Average precipitation	N(8.61, 0.822, min=0 , max=Large)	in/yr	Section 3.1
Average surface runoff	LN(0.0252, 3.33, min=0 , max=0.1)	in/yr	Section 3.1
Average evapotranspiration	N(5.14, 0.762, min=0 , max=Large)	in/yr	Section 3.1
Armor layer moisture content	N(0.125, 0.0175, min=small , max=porosity of Unit 4)	—	Section 3.3, Table 9
Upper filter layer moisture content	same as Armor layer	—	Section 3.3, Table 9
Sacrificial soil moisture content	N(0.243, 0.0175, min=small , max=porosity of silt sand gravel)	—	Section 3.3, Table 9
Lower filter layer moisture content	same as sacrificial soil	—	Section 3.3, Table 9
Water tortuosity water content exponent	U(4/3, 7/3)	—	Section 9.1.3

Parameter	Distribution [*Comments*]	Units	Internal Reference
Water tortuosity porosity exponent	U(0.5, 2)	—	Section 9.1.3
Henry's Law constant ($K_{H,cp}$) for radon	9.3×10^{-3}	mol/L·atm	Section 9.3
Soil temperature	N(12, 1)	°C	Section 9.3
Escape-to-production ratio for uranium in DU oxide wastes	beta(0.290, 0.156, min=0, max=1)	—	Section 9.4.1
Free air diffusivity for radon	0.11	cm^2/s	Section 9.2.2
Thickness of the atmosphere layer	N(μ=2.0, σ=0.5, min=Small, max=Large)	m	Section 9.2.2, Table 15
Wind speed	N(μ=3.14, σ=0.5, min=Small, max=Large)	m/s	Section 9.2.2, Table 15
Atmospheric diffusion length	N(μ=0.1, σ=0.02, min=Small, max=Large)	m	Section 9.2.2, Table 15
Thickness of the Unsat zone (below the embankment clay liner)	N(12.9, 0.25, min=small, max=Large)	ft	Section 7.0
As-Designed Cover			
Mean lateral diversions by upper filter	N(0.0427, 0.0111, min=0, max=Large)	in/yr	Section 3.1
Mean lateral diversions by lower filter	N(3.39, 0.214, min=0 , max=Large)	in/yr	Section 3.1
Mean vertical flow through clay barrier	N(0.104, 0.00417, min=0 , max=Large)	in/yr	Section 3.1
Naturalized Cover			
Time to cover naturalization	N(40, 10, min=10, max=Large)	yr	Section 3.2
Mean lateral diversions by upper filter	0.0	in/yr	Section 3.2
Mean lateral diversions by lower filter	N(0.345, 0.0815, min=small , max=Large)	in/yr	Section 3.2
Mean vertical flow through clay barrier	N(0.0482, 0.00351, min=small , max=Large)	in/yr	Section 3.2
Unit 3			
Porosity_Unit3	equal to MCsat_Unit3	—	Section 4.3
BulkDensity_Unit3	N(ParticleDensity_Unit3 × (1 – Porosity_Unit3), 0.1, min=Small, max=Large)	g/cm^3	Section 4.3
ParticleDensity_Unit3	2.65	g/cm^3	Section 4.3
D_Unit3	N(2.73, 5.21e-3, min=0, max=3)	—	Section 4.4.1

Parameter	Distribution [*Comments*]	Units	Internal Reference
Hb_Unit3	N(8.85, 0.929, min=Small, max=Large); [*correlated to D_Unit3 as -0.85*]	cm	Section 4.4.1
MCres_Unit3	N(6.78e-3, 2.05e-3, min=Small, max=Large); [*truncated just above 0*]	—	Section 4.4.1
MCsat_Unit3	N(0.393, 6.11e-3, min=Small, max=1-Small), [*truncated just above 0 and just below 1*]	—	Section 4.4.1
Ksat_Unit3	N(5.14e-5, 5.95e-6, min=Small, max=Large); [*correlated to D_Unit3 as -0.98*]	cm/s	Section 4.4.1
Unit 4			
Porosity_Unit4	equal to MCsat_Unit4	—	Section 4.3
BulkDensity_Unit4	N(ParticleDensity_Unit4 × (1 – Porosity_Unit4), 0.1, min=Small, max=Large); [*truncated just above 0*]	g/cm^3	Section 4.3
ParticleDensity_Unit4	2.65	g/cm^3	Section 4.3
D_Unit4	N(2.81, 9.93e-5, min=0, max=3)	—	Section 4.4.2
Hb_Unit4	N(104., 1.72, min=Small, max=Large); [*correlated to D_Unit4 as -0.66*]	cm	Section 4.4.2
MCres_Unit4	N(0.108, 8.95e-4, min=Small, max=Large); [*truncated just above 0*]	—	Section 4.4.2
MCsat_Unit4	N(0.428, 6.08e-3, min=Small, max=1-Small); [*truncated just above 0 and just below 1*]	—	Section 4.4.2
Ksat_Unit4	N(5.16e-5, 5.97e-7, min=Small, max=Large); [*truncated just above 0; correlated to D_Unit4 as -0.37*]	cm/s	Section 4.4.2
Fine Cobble Mix			

Parameter	Distribution [*Comments*]	Units	Internal Reference
Porosity_FineCobbleMix	N (0.19, 0.01, min=Small, max=1-Small)	—	Section 5.1.2
BulkDensity_FineCobbleMix	N (ParticleDensity_ FineCobbleMix × (1 – Porosity_FineCobbleMix), 0.1, min=Small, max=Large)	g/cm^3	Section 5.1.2, Section 4.3
ParticleDensity_FineCobbleMix	2.65	g/cm^3	Section 5.1.2, Section 4.3
Fine Gravel Mix			
Porosity_FineGravelMix	N (0.28, 0.01, min=Small, max=1-Small)	—	Section 5.1.4
BulkDensity_FineGravelMix	N (ParticleDensity_FineGravelMix × (1 – Porosity_FineGravelMix), 0.1, min=Small, max=Large)	g/cm^3	Section 5.1.4, Section 4.3
ParticleDensity_FineGravelMix	2.65	g/cm^3	Section 5.1.4, Section 4.3
Rip Rap			
Porosity_RipRap	N (0.18, 0.01, min=Small, max=1-Small)	—	Section 5.1.1
BulkDensity_RipRap	N (ParticleDensity_RipRap × (1 – Porosity_RipRap), 0.1, min=Small, max=Large)	g/cm^3	Section 5.1.1, Section 4.3
ParticleDensity_RipRap	2.65	g/cm^3	Section 5.1.1, Section 4.3
Silt Sand Gravel			
Porosity_SiltSandGravel	N (0.31, 0.01, min=Small, max=1-Small)	—	Section 5.1.3
BulkDensity_SiltSandGravel	N (ParticleDensity_SiltSandGravel × (1 – Porosity_SiltSandGravel), 0.1, min=Small, max=Large)	g/cm^3	Section 5.1.3, Section 4.3
ParticleDensity_SiltSandGravel	2.65	g/cm^3	Section 5.1.3, Section 4.3

Parameter	Distribution [*Comments*]	Units	Internal Reference
Upper Radon Barrier Clay			
Porosity_UpperRnBarrierClay	assigned value for Unit 4	—	Section 4.4.2
BulkDensity_UpperRnBarrierClay	assigned value for Unit 4	g/cm^3	Section 4.3
D_UpperRnBarrierClay	assigned value for Unit 4	—	Section 4.4.2
Hb_UpperRnBarrierClay	assigned value for Unit 4	cm	Section 4.4.2
MCres_UpperRnBarrierClay	assigned value for Unit 4	—	Section 4.4.2
MCsat_UpperRnBarrierClay	assigned value for Unit 4	—	Section 4.4.2
Ksat_UpperRnBarrierClay	LN(5e-8, 1.2)	cm/s	Section 5.1.5
Lower Radon Barrier Clay			
Porosity_LowerRnBarrierClay	assigned value for Unit 4	—	Section 4.4.2
BulkDensity_LowerRnBarrierClay	assigned value for Unit 4	g/cm^3	Section 4.3
D_LowerRnBarrierClay	assigned value for Unit 4	—	Section 4.4.2
Hb_LowerRnBarrierClay	assigned value for Unit 4	cm	Section 4.4.2
MCres_LowerRnBarrierClay	assigned value for Unit 4	—	Section 4.4.2
MCsat_LowerRnBarrierClay	assigned value for Unit 4	—	Section 4.4.2
Ksat_LowerRnBarrierClay	LN(1e-6, 1.2)	cm/s	Section 5.1.6
Generic Waste			
Porosity_Generic_Waste	assigned value for Unit 3	—	Section 4.4.1, Section 6.0
BulkDensity__Generic_Waste	assigned value for Unit 3	g/cm^3	Section 4.3, Section 6.0
D_Generic_Waste	assigned value for Unit 3	—	Section 4.4.1, Section 6.0
Hb_Generic_Waste	assigned value for Unit 3	cm	Section 4.4.1, Section 6.0
MCres_Generic_Waste	assigned value for Unit 3	—	Section 4.4.1, Section 6.0
MCsat_Generic_Waste	assigned value for Unit 3	—	Section 4.4.1, Section 6.0
Ksat_Generic_Waste	assigned value for Unit 3	cm/s	Section 4.4.1, Section 6.0
UO3 Waste			
Porosity_Generic_Waste	assigned value for Unit 3	—	Section 4.4.1, Section 6.0
BulkDensity__Generic_Waste	assigned value for Unit 3	g/cm^3	Section 4.3, Section 6.0
D_Generic_Waste	assigned value for Unit 3	—	Section 4.4.1, Section 6.0

Parameter	Distribution [*Comments*]	Units	Internal Reference
Hb_Generic_Waste	assigned value for Unit 3	cm	Section 4.4.1, Section 6.0
MCres_Generic_Waste	assigned value for Unit 3	—	Section 4.4.1, Section 6.0
MCsat_Generic_Waste	assigned value for Unit 3	—	Section 4.4.1, Section 6.0
Ksat_Generic_Waste	assigned value for Unit 3	cm/s	Section 4.4.1, Section 6.0
U3O8 Waste			
Porosity_Generic_Waste	assigned value for Unit 3	—	Section 4.4.1, Section 6.0
BulkDensity__Generic_Waste	assigned value for Unit 3	g/cm^3	Section 4.3, Section 6.0
D_Generic_Waste	assigned value for Unit 3	—	Section 4.4.1, Section 6.0
Hb_Generic_Waste	assigned value for Unit 3	cm	Section 4.4.1, Section 6.0
MCres_Generic_Waste	assigned value for Unit 3	—	Section 4.4.1, Section 6.0
MCsat_Generic_Waste	assigned value for Unit 3	—	Section 4.4.1, Section 6.0
Ksat_Generic_Waste	assigned value for Unit 3	cm/s	Section 4.4.1, Section 6.0
Liner Clay			
Porosity_LinerClay	assigned value for Unit 4	—	Section 4.4.2
BulkDensity__LinerClay	assigned value for Unit 4	g/cm^3	Section 4.3
D_LinerClay	assigned value for Unit 4	—	Section 4.4.2
Hb_LinerClay	assigned value for Unit 4	cm	Section 4.4.2
MCres_LinerClay	assigned value for Unit 4	—	Section 4.4.2
MCsat_LinerClay	assigned value for Unit 4	—	Section 4.4.2
Ksat_LinerClay	LN(1e-6, 1.2)	cm/s	Section 5.1.7

Porous medium solid/water partition coefficients for various radionuclides in these materials are assigned one of three representative and rather generic collections of K_d values for the materials sand, silt and clay. These assignments are listed in Table 2, with discussion in the relevant sections below. Distributions for the values themselves are documented in the *Geochemical Modeling* white paper.

Table 2. Assignment of solid/water partition coefficients K_d values.

material	K_d material
Unit 2 (includes saturated zone medium)	clay
Unit 3 (includes unsaturated zone medium and all wastes)	sand
Unit 4 (includes loess, clay liner, and upper and lower radon barrier clays)	silt
rip rap	none
fine cobble mix	sand
silt sand gravel	sand
fine gravel mix	sand

2.0 Introduction

Energy*Solutions* operates a low-level radioactive waste (LLW) and mixed waste disposal facility at Clive, Utah. The waste disposal cells (or embankments—the terms are used interchangeably) at the facility are permanent, clay-lined cells with composite caps composed of clay, soil, and cobble layers above the waste. The focus of this white paper is on the hydrologic response of the facility's Class A South (CAS) cell, which has been proposed as a burial site for depleted uranium waste (DU waste). Neptune and Company has been tasked with developing a performance assessment (PA) to evaluate the proposed disposal of DU waste streams in the CAS cell from the Savannah River Site and from the gaseous diffusion plants in Portsmouth, Ohio, and Paducah, Kentucky.

This white paper defines an infiltration model for unsaturated flow through the CAS cell and down to the water table where it enters the saturated zone as recharge. This infiltration model is incorporated into the overall Clive DU PA Model, which is developed using the GoldSim systems analysis modeling software. The infiltration model for the engineered cover is based on calculations for the top and side slopes of the CAS cell that were performed using the EPA's Hydrologic Evaluation of Landfill Performance (HELP) program (Schroeder, et al., 1994). The hydraulic properties for the unsaturated media are based on laboratory measurements by Colorado State University (CSU) for the moisture retention and hydraulic conductivity of core samples from Unit 3 (a silty sand) and Unit 4 (a silty clay) at the site (Bingham Environmental, 1991). The flow analysis determines the suction head, moisture content, and hydraulic conductivity from a solution of the Darcy equation (Buckingham, 1907) for steady state unsaturated flow in the downward direction as a function of vertical infiltration rate.

A detailed description of the hydrogeology of the Clive facility, including the local stratigraphy and construction of the waste cells, has been given in previous reports (Bingham Environmental 1991, 1994) and is not repeated here. Similarly, detailed numerical solutions using the HELP and UNSAT-H modeling programs for infiltration through the engineered cover, waste, clay liners, and soil at the various cells of the facility have been presented in previous reports, most recently for the CAS cell (Whetstone, 2007), and is not repeated here. These reports provide data for analyzing infiltration through the engineered cover and representative soil characteristics for

Units 3 and 4. The latter report also provides numerical results for validating the computational method for solving Darcy's equation that is presented in this white paper.

The infiltration model, soil characteristics, and solution technique for unsaturated flow have been incorporated into the GoldSim-based Clive DU PA Model, for the CAS cell. A major difference between this white paper and the previous work is the effort to incorporate uncertainty in hydrogeologic response into the analysis of unsaturated flow through the CAS cell.

This white paper further describes the contaminant transport mechanisms in unsaturated porous media. This includes gaseous diffusion, water advection and diffusion, and fate and transport of radon.

Section 3.0 defines the infiltration model for the engineered cover on the top and side slopes of the CAS cell's engineered cover. Section 4.0 defines the moisture retention and hydraulic conductivity for Units 3 and 4, based on measurements of core properties by CSU, as well as porosity and bulk density distributions for these materials. Section 5.0 defines the material properties for the engineered materials. Section 6.0 describes material properties for waste materials. Section 7.0 discusses properties of the natural unsaturated zone below the embankment liner and above the water table. Section 8.0 defines the numerical technique for solving Darcy's equation, provides verification of the numerical technique by comparison with results from UNSAT-H, and presents typical results for a range of infiltration rates through the CAS cell. Section 9.0 is devoted to porous medium contaminant transport topics such as advection and diffusion, including the fate and transport of radon in the waste and cover.

3.0 HELP Calculation and Infiltration Model for the Top and Side Slopes

The infiltration model for the engineered cover uses calculations with the HELP program as a guide to defining the vertical and lateral flow rates in the individual layers of the engineered cover as a function of time. The HELP model is a quasi-two-dimensional representation that analyzes the water balance in the cover layers using weather data, soil properties, and landfill design data. The major layers of the as-designed cover and their hydraulic properties are listed in Tables 3 and 4. The names in parentheses under the "Layer No." headings in the Tables are the names of Layers in the PA model. These layers are subdivided into thinner GoldSim Cell Pathway elements, analogous to 1-D finite-difference modeling cells, in the Clive DU PA Model. Differences in construction between the two sections of the cover for the parameters shown are: The porosity of the rip-rap on the top slope is slightly higher than that on the side slope, the hydraulic conductivity of the rip-rap on the side slope is nearly twice that of the rip-rap on the top slope, and the Type-B filter (lower filter) is three times thicker on the side slope than on the top slope.

Table 3. Major layers of the engineered cover on the top slope of the CAS cell.

Layer No.	Material	Thickness	Porosity (-)	K_s (cm/s)	Function	Description
1 (Armor)	Type-B Rip Rap	18 in (~45 cm)	0.19	42	Vertical Percolation	Coarse gravel to fine cobble, 0.75 to 4.5 in
2 (Upper Filter)	Type-A Filter	6 in (~15 cm)	0.19	42	Lateral Drainage	Coarse sand to cobble, 0.08 to 6 in
3	Sacrificial Soil	12 in (~30 cm)	0.31	0.004	Barrier Soil	Silty sand and gravel (coarser than Unit 3)
4 (Lower Filter)	Type-B Filter	6 in (~15 cm)	0.28	3.5	Lateral Drainage	Coarse sand to fine gravel, 0.2 to 1.5 in
5	Upper Radon Barrier	12 in (~30 cm)	0.43	5×10^{-8}	Barrier Soil	Silty clay (Unit 4)
6	Lower Radon Barrier	12 in (~30 cm)	0.43	1×10^{-6}	Vertical Percolation	Silty clay (Unit 4)
7	Waste	100 in (~250 cm)	0.437	5×10^{-4}	Vertical Percolation	Sand
8	Clay Liner	24 in (~60 cm)	0.430	1×10^{-6}	Barrier Soil	Silty clay (Unit 4)

Based on (Whetstone 2007, Table 8)

Table 4. Major layers of the engineered cover on the side slope of the CAS cell.

Layer No.	Material	Thickness (inches)	Porosity (-)	K_s (cm/s)	Function	Description
1 (Armor)	Type-A Rip Rap	18 in (~45 cm)	0.17	80	Vertical Percolation	Coarse gravel to boulders, 2 to 16 in
2 (Upper Filter)	Type-A Filter	6 in (~15 cm)	0.19	42	Lateral Drainage	Coarse sand to cobble, 0.08 to 6 in
3	Sacrificial Soil	12 in (~30 cm)	0.31	0.004	Barrier Soil	Silty sand and gravel (coarser than Unit 3)
4 (Lower Filter)	Type-B Filter	18 in (~45 cm)	0.28	3.5	Lateral Drainage	Coarse sand to fine gravel, 0.2 to 1.5 in
5	Upper Radon Barrier	12 in (~30 cm)	0.43	5×10^{-8}	Barrier Soil	Silty clay (Unit 4)
6	Lower Radon Barrier	12 in (~30 cm)	0.43	1×10^{-6}	Vertical Percolation	Silty clay (Unit 4)
7	Waste	100 in (~250 cm)	0.437	5×10^{-4}	Vertical Percolation	Sand
8	Clay Liner	24 in (~60 cm)	0.430	1×10^{-6}	Barrier Soil	Silty clay (Unit 4)

Based on (Whetstone 2007, Table 9)

Annual water balances for the top and side slopes of the CAS cell computed with the HELP model by Whetstone (2007, Table 12) are shown in Tables 5 and 6.

Table 5. Water balance for the top slope of the CAS cell.

Flow Process	Flow Rate or Head	
Annual Precipitation	22.15 cm/yr	8.72 in/yr
Surface Runoff	0.132 cm/yr	0.052 in/yr
Evapotranspiration	13.1 cm/yr	5.14 in/yr
Lateral Drainage from Type-A (Upper) Filter	0.11 cm/yr	0.043 in/yr
Net Percolation into Sacrificial Soil	8.85 cm/yr	3.483 in/yr (= 8.72 – 0.052 – 5.142 – 0.043)
Head on Top of Sacrificial Soil	0.0025 cm	0.001 in
Lateral Drainage from Type-B (Lower) Filter	8.57 cm/yr	3.374 in/yr
Net Percolation into Upper Radon Barrier	0.277 cm/yr	0.109 in/yr (= 3.483 – 3.374)
Head on Top of Upper Radon Barrier	0.041 cm	0.016 in
Net Percolation through bottom clay layer	0.277 cm/yr	0.109 in/yr

Based on (Whetstone 2007, Table 12, first subtable)

Table 6. Water balance for the side slope of the CAS cell.

Flow Process	Flow Rate or Head	
Annual Precipitation	22.15 cm/yr	8.72 in/yr
Surface Runoff	0.147 cm/yr	0.058 in/yr
Evapotranspiration	12.85 cm/yr	5.058 in/yr
Lateral Drainage from Type-A (Upper) Filter	0.572 cm/yr	0.225 in/yr
Net Percolation into Sacrificial Soil	8.58 cm/yr	3.379 in/yr (= 8.72 – 0.058 – 5.058 – 0.225)
Head on Top of Sacrificial Soil	0.0025 cm	0.001 in
Lateral Drainage from Type-B (Lower) Filter	8.29 cm/yr	3.265 in/yr
Net Percolation into Upper Radon Barrier	0.287 cm/yr	0.113 in/yr (= 3.379 – 3.265)
Head on Top of Upper Radon Barrier	0.005 cm	0.002 in

Based on (Whetstone 2007, Table 12, second subtable)

While there are small differences in the amount of lateral drainage from the upper and lower filter layers for the top and side slope of the cell, the net infiltration entering the upper radon barrier is 0.28 cm/yr (0.11 in/yr) in both cases. Given that net infiltration is essentially the same for both slopes and that the current Clive DU PA Model assumes no placement of waste below the side slope, the infiltration through the engineered cover will be represented with the same

values for both slopes in the GoldSim model. If at a later time modeling will include disposal below the side slope, estimates of infiltration rates for the side slope will be refined.

It is important to note that these deterministic (fixed, constant) values from the HELP modeling were calculated external to GoldSim, not directly in the probabilistic Clive DU PA Model itself. They are used in the development of the uncertain stochastic distributions that are used in the GoldSim model, as developed in subsequent sections, and summarized in Section 1.0, Table 1.

3.1 Cell Infiltration Modeling Approach – As-Designed Condition

Given that the development of the engineered cover over time will likely result in differences in the water balance of the cover, the approach adopted for the PA is to model the cover in its as-designed condition for several decades and then in a condition reflecting development of the materials and colonization by plants for the remaining time period—its "naturalized" condition. Infiltration is assumed to be steady-state.

The calculations for the infiltration model for the as-designed cover are described in Table 7. The input parameter distributions are described in Table 1. The modeled net infiltration and lateral flows are described beginning at the bottom of the cell and moving upwards. For steady-state infiltration, the net infiltration through the upper radon barrier in Layer 5 and through the clay liner in Layer 8 are the same since there are no sources or sinks of water within or between those layers. For example see HELP results for the CAS cell in Table 12 of Whetstone (2007).

The distributions for the net infiltration through the clay liner and lateral flow through the upper and lower filter layers are based on the output of the Whetstone (2007) HELP model. The HELP model simulated 100 years of data. Year 1 results were not included in the analysis in order to avoid the influence of model initial moisture conditions on the calculated annual mean values. The remainder of the data were interpreted as a sample from the underlying distribution for the annual infiltration, except that, since the 100 year simulation time was rather arbitrary, the 99 remaining samples do not necessarily reflect 99 years worth of information. Due to the complexity of the interactions of the inputs, it is not a simple matter to determine how much information is contained in the inputs. Many of the inputs are based on over 100 years of data from the Salt Lake City area. However, due to year-to-year correlation in weather data, these data do not represent 100 independent pieces of information. Therefore, the input information is treated as effectively equivalent to 18 years worth of data (e.g.,the amount of data available for the Clive site).

Since it is the long-term average infiltration rate that is of interest, the distribution represents uncertainty about the mean rate for each of these parameters. While there was some slight right-skewness in the simulated values for each of the three parameters, the uncertainty about the mean is well-represented by a normal distribution. The mean of the normal distribution is set equal to the average simulated value, while the standard deviation of the normal distribution is set equal to the standard error of the mean when treating the simulation as equivalent to 18 years worth of data: the sample standard deviation divided by the square root of 18.

A distribution was developed for the mean annual net infiltration through the clay liner based on 99 mean annual values calculated using the Whetstone HELP model (Whetstone 2007, Appendix

1). Year 1 results were not included in the analysis to avoid the influence of model initial moisture conditions on the calculated annual mean values. The distribution for net infiltration through the clay liner is normal with a mean of 0.264 cm/yr (0.104 in/yr) and a standard deviation of 0.011 cm/yr (0.00417 in/yr). This parameter describes the net infiltration through the upper and lower radon barriers, the waste, the clay liner, and into the unsaturated zone below the cell.

The layer above the upper radon barrier is the lower filter layer (Layer 4). The distribution for lateral flow through the lower filter layer is normal with a mean of 8.61 cm/yr (3.39 in/yr) and a standard deviation of 0.544 cm/yr (0.214 in/yr). The sum of the lateral flow from the lower filter layer and the net infiltration through the clay liner gives the vertical flow through the sacrificial soil in Layer 3 above the lower filter layer.

The layer above the sacrificial soil layer is the upper filter layer (Layer 2). The distribution for lateral flow through the upper filter layer is normal with a mean of 0.108 cm/yr (0.0427 in/yr) and a standard deviation of 0.028 cm/yr (0.0111 in/yr).

Infiltration into Layer 1 (armor) is calculated in the model by subtracting the runoff and evapotranspiration losses from the precipitation.

A probability distribution for precipitation was developed using 12 years of site-specific meteorological data described in Whetstone (2007). Since the parameter of interest is the *mean* annual precipitation, the uncertainty in characterized by a normal distribution with mean equal to the sample mean of 21.9 cm/yr (8.61 in/yr) and standard deviation equal to the sample standard error of 2.09 cm/yr (0.822 in/yr).

The monthly means and standard deviations from HELP model runs listed in Attachment 1 of Whetstone (2007) were utilized as data to develop distributions for runoff and evapotranspiration, following the approach outlined in the *Fitting Probability Distributions* white paper using the mean annual rates from the model runs, with uncertainty propagated across the months to produce standard deviations for the rates. For runoff, the resulting distribution was lognormal with a geometric mean of 0.064 cm/yr (0.0252 in/yr) and a geometric standard deviation of 8.46 cm/yr (3.33 in/yr), with the upper tail truncated at 0.25 cm/yr (0.1 in/yr). The distribution for evapotranspiration was normal with a mean of 13.1 cm/yr (5.14 in/yr) and a standard deviation of 1.94 cm/yr (0.762 in/yr).

Table 7. Infiltration model for top and side slopes of the CAS embankment for the cover as designed.

Layer No.	Material	Flows for as-designed material properties:
1 (Armor)	Type-B Rip Rap	Annual precipitation: distribution from HELP results. Surface runoff: distribution from HELP results. Evapotranspiration (ET): distribution from HELP results. Vertical Flow Armor Layer = Annual Precipitation – Surface Runoff – ET.
2 (Upper Filter)	Type-A Filter	Lateral Flow Upper Filter Layer: distribution from HELP results. Vertical Flow Upper Filter Layer = Vertical Flow Clay Liner + Lateral Flow Lower Filter Layer.

Layer No.	Material	Flows for as-designed material properties:
3	Sacrificial Soil	Vertical Flow Sacrificial Soil = Vertical Flow Clay Liner + Lateral Flow Lower Filter Layer.
4 (Lower Filter)	Type-B Filter	Lateral Flow Lower Filter Layer = distribution from HELP results Vertical Flow Lower Filter Layer = Vertical Flow Clay Liner.
5	Upper Radon Barrier Clay	Vertical Flow Radon Barrier Clay = Vertical Flow Clay Liner.
6	Lower Radon Barrier Clay	Vertical Flow Lower Radon Barrier Clay = Vertical Flow Clay Liner.
7	Waste	Vertical Flow Waste = Vertical Flow Clay Liner.
8	Clay Liner	Vertical Flow Clay Liner: distribution from HELP results.

3.2 Cell Infiltration Modeling Approach – Naturalized Condition

The water balance values for cell layers for the as-designed cover calculated by Whetstone (2007) using HELP are described in Tables 5 and 6. These results demonstrate that evapotranspiration and lateral drainage from the lower filter (Layer 4) provide the main "sinks" that reduce the net infiltration rate into the radon barriers. Assuming that the lower filter layer will remain operational, it follows that changes in evapotranspiration fluxes due to time dependent naturalization of the cover after closure will have the most significant influence on net infiltration. The potential changes in evapotranspiration and lateral drainage as the cover evolves are driven by the following processes:

- Aeolian dust (loess) begins to fill the void spaces between the armor (Layer 1) and the smaller cobbles in the upper filter (Layer 2), providing a soil base for plant (and animal) communities on the top layer of the cover. The dust deposition process is augmented by fracturing of some large cobbles into smaller particles due to weathering. The presence of plants and soil on the cover is expected to increase evapotranspiration, thereby reducing the infiltration into the waste.

  The results of dust deposition, weathering, and plant growth were observed by Neptune and Company staff on the similarly-constructed Vitro cell during an inspection on September 16, 2010. The Vitro cell was closed in December 1988, and provides a site-specific measure of dust deposition, weathering, and plant growth since closure. A partial plant cover of grasses and small shrubs had been established within the past 22 years, based on the growth on the side slope and top slope of the Vitro cell. Based on this information, the time to naturalization of the cover is assigned a normal distribution, with a mean of 40 yr and a standard deviation of 10 yr, truncated with a minimum value of 10 yr.

  Evaporation will likely occur from greater depth once loess fills the void spaces between cobbles in the rip rap and plant cover is reestablished on the top surface of the engineered cover. The measured moisture content in the Cover Test Cell at the site provides evidence for an evaporative zone depth greater than about 45 cm (18 in) (Envirocare

2005). The measured data from the Cover Test Cell show that the middle of the sacrificial soil, at a depth of 76 cm (30 in) below the top of the cover, experiences seasonal drying during the six months with very low precipitation at the site (Envirocare 2005, Figures 3 and 4). Some of this drying is due to evapotranspiration, although drainage to the underlying clay layers (i.e., the radon barrier) may also play a role.

- Although burrowing mammals and ants will cause some bioturbation, they are not expected to populate the engineered cover in sufficient numbers to cause homogenization of the armor and upper filter (Layers 1 and 2). It is likely that smaller mammals may burrow a bit in the silted rip rap, but would not find the underlying cobbles hospitable compared to the virgin soil surrounding the embankment. It is also unlikely that ants will find sufficient room amongst the cobbles and gravel to build satisfactory chambers in Layers 1 and 2.
- The lower layers of the engineered cover, Layers 3 and 4, will be a good habitat for deeper plant roots, based on a biological survey of the site. Observations made during a biological survey at the Clive facility (SWCA, 2011) indicate that plant roots often form on top of clay layers that are a meter or more below the top surface, such as the upper radon barrier (Layer 5). Some of these roots may penetrate the radon barriers, based on observations of plant roots in clay layers in boring logs. However, Energy*Solutions* excavated into the first clay unit in the shallow subsurface and observed that the roots did not appear to penetrate the clay, but rather, spread and stayed in the more silty sandy unit above the clay. It is possible that ants may also penetrate the clay layers by following root holes or possible cracks in the clay layers. On balance, the evidence suggests that bioturbation and homogenization of the radon barriers will probably occur very slowly relative to the 10,000-yr time frame for the quantitative part of the PA.

To simulate the performance of the cover system as the designed system is affected by natural forces and becomes colonized by vegetation, several changes were made to the properties of the upper two layers to represent their long-term characteristics. The rip-rap layer and upper filter layer porosity are assumed to be filled with loess within a few decades after closure. Layer 1 as designed is 45 cm (18 in) thick, with a design porosity of 0.19. Layer 2 as constructed is 15 cm (6 in) thick composed of coarse sand, coarse gravel and cobbles, also with a design porosity of 0.19. There is then an equivalent 60 cm (24 in) × 0.19 = 11.7 cm (4.6 in) of available pore space that will be filled with loess. For the HELP model of the naturalized cover, these two layers will be replaced with a single equivalent layer of soil 11.7 cm (4.6 in) thick, having the characteristics of the surface soils in the vicinity of the cell.

The sacrificial soil layer in the HELP model of the as-designed cover is located directly below the upper filter layer, a lateral drainage layer. Since HELP cannot model capillary flow across the filter layer, the soil layer had to be classified as a barrier soil liner. In HELP, a barrier layer is assumed to be saturated at all times and allows flow only when there is a positive head on the top surface. HELP allows only downward saturated flow in barriers and no evapotranspiration. By combining the upper two layers into an equivalent soil layer, the sacrificial soil layer can be re-classified in the HELP model as a vertical percolation layer, and the evaporative zone can be extended to the top of the lower filter layer. Values of field capacity and wilting point moisture content data for both soils were obtained from the National Resources Conservation Service Web

Soil Survey (USDA, 2011). The average wilting point and field capacity weighted by area are 0.286 and 0.148 respectively (see Section 3.3). An average value of saturated hydraulic conductivity from the NRCS Web Soil Survey (USDA, 2011) was reported as 2.2×10^{-4} cm/s for both soils. A value of 0.5 was used for the total porosity considering the mean porosity of unit 4 soil cores of 0.43 and some porosity increase due to the presence of vegetation. An initial value for moisture content of 0.13 was used for the sediment filled layer and for the sacrificial soil layer. This value is the mean of the distribution for moisture content estimated for the upper soil layers described in Section 3.3 below. The lower filter layer was assumed to remain functional.

Vegetation was included in the system, described in HELP as "a poor stand of grass" with an evaporative zone depth of 42.2 cm (16.6 in). A leaf area index of 1.26 was assigned to the vegetation corresponding to the value used for cheatgrass by Ward et al. (2005) for an area on the Hanford site in eastern Washington.

For estimating runoff, the upper surface was characterized as bare gravel for the as-designed cover. These inputs were changed to a HELP default soil texture of 9 representing a silt loam soil (Schroeder et al. 1994) and a vegetation index of 2, representing a "poor stand of grass" as described in the HELP User's Guide (Schroeder et al. 1994).

The HELP model was run for 100 years with these changes in structure and inputs and the mean annual flows from the lower filter layer and net infiltration from the clay liner were used to develop distributions for the GoldSim model as described previously for the as-designed condition. The distribution for lateral flow in the lower filter layer is normal with a mean of 0.876 cm/yr (0.345 in/yr) and a standard deviation of 0.207 cm/yr (0.0815 in/yr). The distribution for the mean annual net infiltration through the clay liner is normal with a mean of 0.122 cm/yr (0.0482 in/yr) and a standard deviation of 0.0089 cm/yr (0.00351 in/yr). Since the upper filter layer is assumed to have been silted up and is therefore ineffective at diverting infiltrating water, it is assigned a lateral flow of 0 cm/yr (0 in/yr).

Comparisons of HELP modeling results with results from mechanistic unsaturated zone modeling programs such as UNSAT-H at arid and semi-arid sites suggest that the HELP model will generally overestimate the net infiltration through the waste in the CAS cell (Meyer et al. 1996, Khire et al. 1997, Albright et al. 2002). The results from the calculation with the HELP model for the CAS cell provide a reasonable estimate of the steady-state infiltration for the PA model.

3.3 Embankment Layer Moisture Contents

GoldSim uses Cell Pathway Elements to model compartments in the 1-D contaminant transport columns. Part of the definition of each Cell is the specification of the amount of various materials in the Cell, including the volume of water. It is therefore necessary to determine the volume of water that should be specified for each Cell in the column, and this is done by knowing the entire volume of the Cell, and multiplying by the water (moisture) content of the porous material in it. This section discusses the determination of moisture contents in the various model layers and materials.

The radionuclide transport and diffusion calculations in the Clive DU PA Model require the moisture content of layers 1 through 4 that are described in Tables 3 and 4, as well as the net

infiltration rates, described previously in Sections 3.1 and 3.2. Calculation of moisture contents for the upper radon barrier and underlying layers is discussed in Section 8.3. In assigning probability distributions for moisture content, layers 1 and 2 (armor layer and upper filter) were combined, since loess is expected to infill both layers. Likewise, layers 3 and 4 (sacrificial soil and lower filter) were combined. Natural Resource Conservation Service mapping of the site indicated that approximately 85 percent of the soils on and near the site were classified as the Skumpah series and the remaining 15 percent as the Timpie series (USDA, 2011). Field capacity and wilting point moisture content data for both soils obtained from (USDA, 2011) are shown in Table 8. The average wilting point and field capacity weighted by area are 0.148 and 0.286 respectively. Daily precipitation data were used to estimate the fraction of time the soil would be at a moisture content corresponding to the wilting point and the fraction of time the soil would be at a moisture content corresponding to field capacity. These fractions, combined with the average wilting point and field capacity moisture contents, provide an estimate of the mean moisture content over time. The precipitation data set was then divided into six equal periods and each period was analyzed in the same manner as the entire data set to obtain an estimate of the standard deviation. The resulting distributions for moisture content for layers 1 through 4 are summarized in Table 9.

Table 8: Wilting point and field capacity water contents for Skumpah and Timpie Soil Series.

Soil Series	Wilting Point Water Content	Field Capacity Water Content
Skumpah	0.154	0.288
Timpie	0.115	0.272

Table 9. Moisture contents in layers 1 through 4 of the top slope and side slope cover.

Layer No.	Material	Moisture Content Distribution
1 (Armor)	Rip Rap	Normal distribution with a mean of 0.125 and a standard deviation of 0.0175.
2 (Upper Filter)	Type-A Filter	
3 (Sacrificial Soil)	Sacrificial Soil	Normal distribution with a mean of 0.243 and a standard deviation of 0.0175.
4 (Lower Filter)	Type-B Filter	

4.0 Soil Characteristics of Unit 3 and Unit 4

4.1 Laboratory Measurements

The hydraulic properties for Units 3 and 4 are based on laboratory measurements by CSU for the moisture retention and hydraulic conductivity of core samples from Units 3 and 4 at the Clive site (Bingham Environmental 1991). Measurements of water retention as a function of matric pressure (called suction head in this report) are available for the drying and wetting cycles. These measurements were performed on four cores: GW19A-B1 and GW17A-B2 from Unit 4 (a silty clay), and GW18-B4 and GW17A-B5 from Unit 3 (a silty sand). Measurements of hydraulic

conductivity as a function of moisture content are available for three cores: GW19A-B1, GW18-B4, and GW17A-B5. The focus in this work (and in previous work) is on the wetting cycle data because infiltration after a heavy rain, which is a major driver for downward flow and transport, is driven by a rewetting front that passes through the engineered cover, waste, and clay layers. The Appendix documents the hydraulic data for Units 3 and 4, based on data reported in (Bingham Environmental 1991, pp. B-19 through B-31).

4.2 Grain Size Distributions for the Cores

Tables 10 and 11 summarize the grain size distributions according to the Unified Soil Classification System (Bingham Environmental, 1991) for cores from Units 4 and 3, respectively. Table 10 is sorted by increasing percent of clay plus silt content. Table 11 is sorted by increasing percent of sand content. The four cores that were tested by CSU have the following properties:

- GW17A-B2 has 55.6% clay, the highest measured clay content with a trace of sand in Table 10 for Unit 4,
- GW19A-B1 has 56.2% silt, the highest measured silt content with a trace of sand in Table 10 for Unit 4,
- GW18-B4 has 45.5% sand, the lowest measured sand content in Table 11 for Unit 3, and
- GW17A-B5 has 83.3% sand, the highest measured sand content in Table 11 for Unit 3.

The core samples that were selected for testing span the extremes of the clay, silt, and sand contents for Units 3 and 4. The core samples that were tested are in a bold font in Tables 10 and 11.

The water retention data are consistent with these material distributions, as shown in Figure 1. In particular, the core that has the greatest clay content retains a greater moisture content than the cores that are high in silt or sand at a given suction head, and the core that has the greatest sand content demonstrates the abrupt changes in moisture content that are typical of a sandy material.

Table 10. Grain size distributions for cores* from Unit 4, a silty clay.

Well/Sample No.	Depth (ft)	Description	% Gravel	% Sand	% Silt	% Clay	% Clay + Silt	Reference
I-3-50 (SE)	1.5	Silty Clay	0	39.3			60.7	Bingham 1994, page 23
I-4-50 (SE)	10.5	Silty Clay	0	19.6			80.4	Bingham 1994, page 32
I-3-50 (SE)	10.5	Silty Clay	0	16.6			83.4	Bingham 1994, page 24
I-1-50 (NW)	7.5	Silty Clay	0	11.7			88.3	Bingham 1994, page 13
GW-16/S-1	3 - 5	Brown Silty Clay w/Trace Fine Sand	0.1	11.2	50.3	38.4	88.7	Bingham 1991, page B-13
GW-19A/S-1	**5-7**	**Brown Silty Clay w/Trace Fine Sand**	**0**	**2.8**	**56.2**	**41.0**	**97.2**	**Bingham 1991, page B-17**

Well/Sample No.	Depth (ft)	Description	% Gravel	% Sand	% Silt	% Clay	% Clay + Silt	Reference
GW-17A/L-2	**7-9.5**	**Brown Silty Clay w/Trace Fine Sand**	**0**	**2.1**	**42.3**	**55.6**	**97.9**	**Bingham 1991, page B-15**
GW-18/B-1	5-6.5	Brown Silty Clay w/Trace Fine Sand	0	2.0	49.9	48.1	98.0	Bingham 1991, page B-16
I-4-50 (SE)	7.5	Silty Clay	0	1.2			98.8	Bingham 1994, page 31

*Cores in bold font were tested by CSU

Table 11. Grain size distributions for cores* from Unit 3, a silty sand.

Well/Sample No.	Depth (ft)	Description	% Gravel	% Sand	% Silt	% Clay	% Clay + Silt	Reference
GW-18/S-4	**20-22**	**Brown Silty Fine Sand w/Some Clay**	**0**	**45.5**	**38.7**	**15.8**	**54.5**	**Bingham 1991, page B-16**
I-1-50 (NW)	18.0	Silty Sand	0	48.2			51.8	Bingham 1994, page 15
DH-48/B-2	17-19	Tan Silty Sand	0	55.5			44.5	Bingham 1994, page B-11
GW-16/B-4	19.5-21	Tan Silty Fine Sand	0	59.4			40.6	Bingham 1991, page B-14
I-3-50 (SE)	19.5	Silty Sand	0	62.3			37.7	Bingham 1994, page 26
GW-41/B-6	10-12	Tan Silty Sand	0	65.3			34.7	Bingham 1994, page B-10
GW-41/B-9	16-18	Tan Silty Sand	0	66.3			33.7	Bingham 1994, page B-10
I-1-50 (NW)	10.5	Silty Sand	0	66.6			33.4	Bingham 1994, page 14
GW-19B/B-4	17-19	Tan Silty Fine Sand	0	66.7			33.3	Bingham 1991, page B-18
GW-55/B-8	14-16	Tan Silty Sand	1.1	69.5			29.4	Bingham 1994, page B-11
DH-33/L-7	16.5	Tan Silty Sand	0.1	72.9			27	Bingham 1994, page B-9
GW-16/B-3	14.5-16	Tan Silty Fine Sand	0.2	74.7			25.1	Bingham 1991, page B-13
I-3-50 (SE)	15	Silty Sand	0	75.8			24.2	Bingham 1994, page 25
I-4-50 (SE)	21	Silty Sand	0	76.4			23.6	Bingham 1994, page 33

Well/Sample No.	Depth (ft)	Description	% Gravel	% Sand	% Silt	% Clay	% Clay + Silt	Reference
GW-16/B-2	9.5-11	Tan Silty Fine Sand	1.6	79.8			18.6	Bingham 1991, page B-13
GW-19A/S-3	15-16	Brown Silty Fine Sand	0	82.0			18	Bingham 1991, page B-17
GW-17A/L-5	**19.5-22**	**Brown Silty Fine Sand w/Trace Clay**	**0**	**83.8**	**8.4**	**7.8**	**16.2**	**Bingham 1991, page B-15**
GW-19B/L-5	22-24.5	Tan Silty Fine Sand	0	83.8			16.2	Bingham 1991, page B-18

*Cores in bold font were tested by CSU

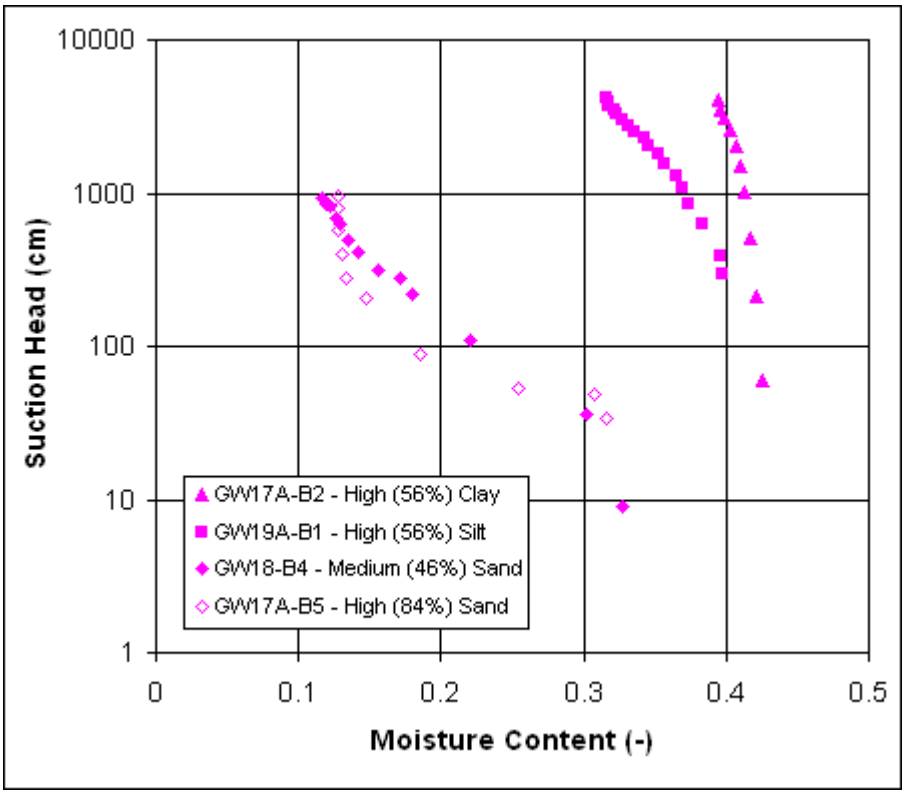

Figure 1. Comparison of water retention data (wetting cycle) for four core samples

4.3 Soil Material Properties

Particle density ρ_s is defined as the ratio of the mass of the solid to the volume of the solid:

$$\rho_s = M_{solid} / V_{solid}.$$

Particle density depends on the chemical composition and crystalline structure of the mineral particles. Particle density is not influenced by particle size, packing arrangement, or pore space.

Dry bulk density ρ_b is defined as the ratio of the mass of dried alluvium to its total volume,

$$\rho_b = M_{solid} / V_{total}.$$

For a dried sample, $V_{total} = V_{solid} + V_{gas}$.

Porosity, ϕ, (often also denoted as n) is the relative pore volume of the medium,

$$V_{liquid} + V_{gas} / V_{solid} + V_{liquid} + V_{gas}.$$

For a dry sample, porosity is $V_{gas} / (V_{solid} + V_{gas})$. Total porosity can be determined from dry bulk density and particle density by $\phi = 1 - \rho_b / \rho_s$. Therefore, relating these equations,

$$\phi = 1 - \rho_b / \rho_s = (\rho_s - \rho_b)/\rho_s = [\, M_{solid} / V_{solid} - M_{solid} / (\, V_{solid} + V_{gas}\,)\,] / (\, M_{solid} / V_{solid}\,) = V_{gas} / (\, V_{solid} + V_{gas}\,)$$

The structure of coarse dry alluvium is generally single grained. The actual packing arrangement depends on grain size distribution, grain shape, and the processes under which the alluvium was deposited. The grain size distribution can consist of a single grain size (monodisperse) or multiple grain sizes (polydisperse). The packing arrangements of spherical grains of uniform size can be represented by models for regular packing that allow the calculation of the spacing of layers, the volume of a unit cell and thus the bulk density. Although monodisperse systems are idealizations of natural porous materials such as alluvium, calculated relationships between particle density and bulk density gives some insight into potential particle density – bulk density correlation. The unit cell volume, bulk density, and porosity are given in the table below for for five models of regular packing of uniform spheres.

Table 12. Theoretical porosities based on particle packing geometry.

Model	Unit Cell Volume (*R* is grain radius)	Bulk Density	Porosity
simple cubic	$8R^3$	$\Pi\rho_s/6$	47.64
cubic tetrahedral	$4\sqrt{3}\ R^3$	$\Pi\rho_s/3\sqrt{3}$	39.54
tetragonal sphenoidal	$6R^3$	$2\Pi\rho_s/9$	30.19
pyramidal	$4\sqrt{2}R^3$	$\Pi\rho_s/3\sqrt{2}$	25.95
tetrahedral	$4\sqrt{2}R^3$	$\Pi\rho_s/3\sqrt{2}$	25.95

Source: Deresiewicz (1958, Table 1) reported in Hillel (1980, Table 6.1)

These calculations show that the bulk density of a volume of monodisperse spheres of constant particle density depends on the packing arrangement. Thus, correlation between particle density and bulk density would only be expected for a sample characterized by a single packing arrangement.

Polydisperse systems are more complex with grains of smaller radii filling in the pore spaces between larger grains. The increase in bulk density due to infilling by smaller particles depends on the grain size distribution. Natural materials are more likely to be characterized by a range of

particle sizes leading to many diverse packing arrangements. The large range of possible packing arrangements in coarse alluvium makes a physically based correlation between particle density and bulk density unlikely.

Given the conclusion that particle density and bulk density are not physically dependent and given the need to restrict the sampling of material properties and moisture content parameters to physically meaningful and consistent values the following approach was taken:

1) Separate up-scaled distributions for Unit 3 and 4 for saturated water content and residual water content are estimated from borehole water retention curve and hydraulic conductivity data. This estimation approach is detailed in subsequent sections.

2) Porosity is assumed to be equal to the saturated water content.

3) Based on particle density data presented in Table 13 and best professional judgement a constant value of 2.65 g/cm^3 was chosen for particle density for both Unit 3 and 4, fine cobble mix, fine gravel mix, rip rap, silt sand gravel.

4) Based on bulk density data presented in Table 13 and best professional judgement an up-scaled distribution for bulk density was specified as a normal distribution with a mean of (1- porosity) times particle density and a standard deviation of 0.1. This was applied to both Unit 3 and 4, fine cobble mix, fine gravel mix, rip rap, silt sand gravel..

This approach allows the uncertainty in water content and bulk density to be modeled while maintaining a physically coherent probabilistic unsaturated zone model.

Table 13: Bulk density, porosity, and calculated particle density data from water retention experiments.

Borehole	Unit	Bulk Density (g/cm)	Porosity	Calculated Particle Density (g/cm^3)
GW18-B4	3	1.567	0.409	2.65
GW17A-B5	3	1.673	0.32	2.46
GW19A-B1	4	1.397	0.473	2.65
GW17A-B2	4	1.326	0.505	2.68

from Colorado State University Porous Media Laboratory

4.4 Soil Moisture Content

The flow of water in porous media occurs in response to a gradient in the total potential energy of water. The total potential can be composed of a number of components but this analysis will be restricted to gravitational and matric potentials. Water potential components are often expressed in units of energy per unit weight rather than units of energy per unit mass. When the quantity of water is expressed as a weight, the units of potential are defined in terms of head. The gravitational potential refers to the energy of water with respect to reference elevation and is written here as Z. Although not a formal definition, the matric potential relates to the energy of

the tension imposed on the pore water by the soil matrix. Matric potential is a negative value and is written here as ψ. The total potential is then $H = \psi + Z$.

Steady-state fluid flow in an unsaturated medium is defined by the Buckingham-Darcy equation (Jury and Horton, 2004, p.95). In the following discussion this equation will be referred to simply as the Darcy equation. The one dimensional form of Darcy's equation for unsaturated flow is given by Fayer (2000, Eqns. 4.2 and 4.5):

$$q = -K_L(\psi)\frac{\partial H}{\partial z}, \tag{1}$$

where

- q is the flux of liquid per unit area,
- K_L is the unsaturated conductivity as a function of the matric head ψ,
- H is the matric plus gravitational potentials [cm], and
- z is the depth below ground surface [cm].

It is convenient to define two sign conventions for the total potential (Fayer 2000, page 4.2): (1) the z-coordinate is zero at the soil surface and positive downward. With this convention, the gravitational head in the soil, which is defined as the elevation of a point with respect to the soil surface, and negative and defined as $-z$; and (2) the suction head, h, is the negative of the matric potential or matric head, ψ. With this convention, the suction head, h, is always greater than zero for an unsaturated soil. It follows that

$$H = \psi + Z = -(h + z) \tag{2}$$

and the flux is then given by

$$q = K_L(h)\left(\frac{\partial h}{\partial z} + 1\right). \tag{3}$$

The unsaturated conductivity, K_L, is formulated based on the Brooks-Corey representation for moisture content as a function of suction head

$$\begin{aligned} \Theta &= \left(\frac{h}{h_b}\right)^{-\lambda} \quad for\ h > h_b, \\ &= 1 \qquad for\ 0 \le h \le h_b \end{aligned} \tag{4}$$

where

- Θ is the effective saturation,
- h is the suction head (cm),
- h_b is the bubbling pressure head (cm) at which moisture first drains from the material, and
- l is a constant that is fit to data.

Alternatively, expressed in terms of the fractal dimension, D

$$\Theta = \left(\frac{h}{h_b}\right)^{D-3} \quad for\ h > h_b, \qquad = 1 \quad for\ 0 \le h \le h_b \tag{5}$$

The suction head is positive for an unsaturated material and 0 at saturation. Θ, the effective saturation, is defined as

$$\Theta = \frac{\theta - \theta_r}{\theta_s - \theta_r}, \tag{6}$$

where

- Θ is the moisture content,
- Θ_r is the residual moisture content, and
- Θ_s is the saturated moisture content.

Combining Equations

$$\theta = \theta_r + \left(\theta_s - \theta_r\right)\left(\frac{h}{h_b}\right)^{-\lambda} \tag{7}$$

This equation can then be fit to core data.

Alternatively, expressing in terms of D and assuming

$$\theta = \theta_r + (\theta_s - \theta_r)\left(\frac{h}{h_b}\right)^{(D-3)} \tag{8}$$

Using the Mualem theory for predicting hydraulic conductivity (Mualem 1976), the unsaturated hydraulic conductivity is defined as

$$K_L = K_S \Theta^{2+\frac{2}{\lambda}}. \tag{9}$$

Substituting Equation 6 into Equation 9 gives:

$$K_L = K_S \left(\frac{\theta - \theta_r}{\theta_s - \theta_r}\right)^{2+\frac{2}{\lambda}}. \tag{10}$$

Setup (e.g. unit 3)

1) from 4 measurements estimate mean and standard error for porosity (ϕ) and θ_r, use these as priors for θ_s and θ_r (assumes $\theta_s = \phi$).
2) for each borehole core there are 2 separate measurements
    1. moisture content, θ; and suction head, h

2. moisture content, θ; and hydraulic conductivity K_L
3. estimate h_b, D, θ_s, θ_r, and K_s as described below

Here's the Brooks-Corey $\theta \sim f(h)$ equation:

$$\theta = \theta_r + (\theta_s - \theta_r)\left(\frac{h}{h_b}\right)^{(D-3)} \tag{11}$$

Here's $K_L \sim f(\theta)$

$$K_L = K_S\left(\frac{\theta - \theta_r}{\theta_s - \theta_r}\right)^{-(\tau + 2/(D-3))} \tag{12}$$

where the data are

θ	the water content,
h	is the suction head (cm),
K_L	is hydraulic conductivity (cm/sec),

and the parameters to be fit are

h_b	is the air entry pressure head (cm),
D	is the soil fractal dimension,
θ_s	is the saturated water content,
θ_r	is the residual water content,
τ	is the Mualem empirical parameter = 2,
K_S	is saturated hydraulic conductivity (cm/sec),

Typically these relationships are fit using non-linear least squares. However, it seems for these boreholes the optimization has trouble converging and the uncertainty in parameter estimates is difficult to estimate. To allow combining of information available across the available borehole moisture content and hydraulic conductivity datasets and to provide an estimate of the uncertainty in these parameter estimates a Bayesian Markov Chain Monte Carlo (MCMC) simulation approach was taken that allows the parameters to be constrained via prior distributions and generates parameter posterior distributions. This also allows the two sets of information from a borehole to be combined as well as allowing for combing information across boreholes for a unit (borehole data are presented in the Appendix).

In a Bayesian approach sources of information on model parameters can be combined through a prior distribution or through a data likelihood. The priors integrate expert judgment and scientific knowledge while the likelihood integrates information available in observed data. In effect, the prior can be used to constrain the results parameter distribution to physical meaningful values.

The priors listed below (Equations 13-19) are all non-informative distributions which allow the data to determine the distribution and also constrain the parameter values to a physically meaningful range.

$$p(\theta_s) = U[0.3, 0.55] \tag{13}$$

$$p(\theta_r) = U[0.001, 0.2] \tag{14}$$

$$p(h_b) = U[1, 500] \tag{15}$$

$$p(D) = U[1, 2.999] \tag{16}$$

$$p(\sigma) = U[0.001, 1000] \tag{17}$$

$$p(K_{sat}) = U[\text{10e-10}, \text{10e-3}] \tag{18}$$

$$p(\sigma_{K_s}) = U[\text{1e-9}, \text{1e-4}] \tag{19}$$

and the likelihood based on the moisture content matrix pressure data:

$$\begin{aligned} p(\theta_s, h_b, D, \sigma \mid \theta_{borehole1}, \theta_{borehole2}, h_{borehole1}, h_{borehole2}) = \\ N_{borehole1}\left[\theta_r + (\theta_s - \theta_r)\left(\frac{h_{borehole1}}{h_b}\right)^{(D-3)}, \sigma\right] \\ N_{borehole2}\left[\theta_r + (\theta_s - \theta_r)\left(\frac{h_{borehole2}}{h_b}\right)^{(D-3)}, \sigma\right] \end{aligned} \tag{20}$$

and the likelihood based on the moisture content hydraulic conductivity data:

$$\begin{aligned} p(\theta_s, \theta_r, D, K_S, \sigma_{K_s} \mid \theta_{borehole1}, \theta_{borehole2}, K_{L_{borehole1}}, K_{L_{borehole2}}) = \\ N_{borehole1}\left[K_S\left(\frac{(\theta - \theta_r)}{(\theta_s - \theta_r)}\right)^{-(2+2/(D-3))}, \sigma_{K_s}\right] \\ N_{borehole2}\left[K_S\left(\frac{(\theta - \theta_r)}{(\theta_s - \theta_r)}\right)^{-(2+2/(D-3))}, \sigma_{K_s}\right] \end{aligned} \tag{21}$$

Markov Chain Monte Carlo (MCMC) simulation of the joint distribution define by equations 13-21 was used to generate samples from the marginal parameter distributions for the moisture content and hydraulic conductivity models. Results for Unit 3 and 4 are presented in the following sections.

4.4.1 Unit 3 Brooks-Corey Parameters

The MCMC sampling using likelihoods incorporating the two Unit 3 borehole cores resulted in the the following marginal parameter distributions:

$$p(h_b) = N[mean = 8.85, sd = 0.929] \tag{22}$$

$$p(D) = N[mean = 2.73, sd = 5.21\text{e-}3] \quad (23)$$

$$p(K_S) = N[mean = 5.14\text{e-}05, sd = 5.95\text{e-}6] \quad (24)$$

$$p(\theta_s) = N[mean = 0.393, sd = 6.11\text{e-}03] \quad (25)$$

$$p(\theta_r) = N[shape = 6.78\text{e-}3, scale = 2.05\text{e-}3] \quad (26)$$

Significant correlations from these simulations was found between D and H_b (-0.85) and between K_{sat} and D (-0.98).

4.4.2 Unit 4 Brooks-Corey Parameters

The MCMC sampling using likelihoods incorporating the two Unit 4 borehole cores resulted in the the following marginal parameter distributions:

$$p(h_b) = N[mean = 104., sd = 1.72] \quad (27)$$

$$p(D) = N[mean = 2.81, sd = 9.93\text{e-}5] \quad (28)$$

$$p(K_S) = N[mean = 5.16\text{e-}05, sd = 5.97\text{e-}7] \quad (29)$$

$$p(\theta_s) = N[mean = 0.428, sd = 6.08\text{e-}3] \quad (30)$$

$$p(\theta_r) = N[shape = 0.108, scale = 8.95\text{e-}4] \quad (31)$$

Significant correlations from these simulations was found between D and H_b (-0.66) and between K_{sat} and D (-0.37).

5.0 Engineered Materials

The cap over the facility is constructed of engineered materials that are derived from natural materials. These generally consist of various grades of sorted aggregates, or of clay compacted to specific tolerances. Properties for these materials are described in Whetstone (2000, Tables 7 and 8).

5.1.1 Rip Rap

Rip Rap is used to construct the uppermost layer: Armor. The Rip Rap itself is assumed to be an inert material. The Class A South cover design (EnergySolutions, 2009, drawing 07021 V7) assigns Type A rip rap to the side slopes, and Type B rip rap to the top slope, we have adopted common properties for the two types for the purposes of this assessment. This is justified, since the only role of the rip rap in the dimensional and hydraulic properties of the cap is to take up space as an inert material. In that sense, it is sufficient to average the two porosities of 0.17 and 0.19, for Types A and B respectively (Whetstone, 2000, Tables 7 and 8), to be 0.18, with a standard deviation of 0.01, so that the range is suitably covered.

As the pore space of the rip rap becomes becomes infilled with loess within decades after closure, the original porosity of the rip rap takes on the properties similar to the Unit 4 soil (Section 3.2).

5.1.2 Fine Cobble Mix

Fine Cobble Mix is used to construct the upper filter layer. Distributions for the as-designed upper filter layer (fine cobble mix) parameters are described in Table 1. The Fine Cobble Mix

itself is assumed to be an inert material. As the pore space of the upper filter layer becomes infilled with loess within decades after closure, the original porosity of the upper filter layer takes on the properties similar to the Unit 4 soil (Section 3.2).

5.1.3 Silt Sand Gravel

Silt Sand Gravel is used to construct the sacrificial soil layer. Distributions for the sacrificial soil layer (silt sand gravel) parameters are described in Table 1. Properties of the sacrificial soil layer are not expected to change with time.

5.1.4 Fine Gravel Mix

Fine Gravel Mix is used to construct the lower filter layer. Distributions for the lower filter layer (fine gravel mix) parameters are described in Table 1. The lower filter layer is assumed to remain operational during the modeled time period. The Fine Gravel Mix itself is assumed to be an inert material.

5.1.5 Upper Radon Barrier Clay

The Radon Barrier layers are divided into upper and lower layers. Both are constructed of local clay, compacted to different hydraulic conductivities. UpperRnClay represents the upper of the two layers. Distributions for upper radon barrier clay parameters are described in Table 1. The distribution for saturated hydraulic conductivity was developed using the design value (Table 3) for the clay layer of 5×10^{-8} cm/s as the geometric mean of a lognormal distribution. A geometric standard deviation of 1.2 was chosen to provide an approximate order of magnitude variation above and below the geometric mean.

5.1.6 Lower Radon Barrier Clay

The Lower Radon Barrier is constructed of compacted local clay. LowerRnClay represents the lower of the two layers. Distributions for the lower radon barrier clay parameters are described in Table 1. The distribution for saturated hydraulic conductivity was developed using the design value (Table 3) for the clay layer of 1×10^{-6} cm/s as the geometric mean of a lognormal distribution. A geometric standard deviation of 1.2 was chosen to provide an approximate order of magnitude variation above and below the geometric mean.

5.1.7 Liner Clay

The Liner is constructed of compacted local clay, here defined as LinerClay. Distributions for the liner clay parameters are described in Table 1. The distribution for saturated hydraulic conductivity was developed using the design value (Table 3) for the clay layer of 1×10^{-6} cm/s as the geometric mean of a lognormal distribution. A geometric standard deviation of 1.2 was chosen to provide an approximate order of magnitude variation above and below the geometric mean.

6.0 Porous Media Properties of Waste Materials

Test data are not available for the unsaturated porous media properties of the wastes. However, the DU waste is expected to be in a powdered form or possibly compressed into small "briquettes" for safety during transportation to the Clive facility. In this condition, the DU waste will behave like a mixture of fine sand to fine gravel. Since there is so little information on which to base material properties for the waste, it is assigned the properties of Unit 3.

Three types of waste materials are considered in the DU PA: Generic LLW, the UO_3 waste from the SRS, and the U_3O_8 wastes from the gaseous diffusion plants (GDPs) at Portsmouth, OH, and Paducah KY. The generic LLW is used only as an inert filler in the model, with no inventory, and is assumed to simply have the properties of local silty sandy soil: Unit 3.

The uranium oxide wastes, both UO_3 and U_3O_8, will be disposed in an indeterminate mix of materials, including containers (55-gallon drums and DU cylinders of various types) and possibly concrete, grout, bulk LLW, and local soils as backfill. This complex mix of heterogeneous materials is not modeled at this point, and the assumption is made instead that the overall material properties are again simply that of local silty sandy soil: Unit 3.

So, in summary, all waste materials in the Clive DU PA Model are assumed to have the same physical properties as Unit 3 soils.

7.0 Properties of the Natural Unsaturated Zone

The CAS embankment is constructed by excavating through the uppermost stratum, Unit 4, and into the top of Unit 3. The entire unsaturated zone below the embankment, from the bottom of the clay liner to the top of the saturated zone, is modeled as Unit 3 material, sharing all the properties and characteristics of Unit 3 as outlined in this white paper. The saturated zone is modeled as Unit 2 (see the *Saturated Zone Modeling* white paper). In the GoldSim PA Model, this zone below the embankment is called the Unsat zone, and does not include overlying waste and cover materials. It is part of both the top slope and side slope columns.

The thickness of the Unsat zone below the CAS is determined by the difference in average elevations of the bottom of the clay liner and the water table. The clay liner is uniformly about 60 cm (2 ft)-thick by design, though the bottom of the waste cell has a gentle slope to it, as documented in the *Embankment Modeling* white paper.

A distribution for the thickness of the unsaturated zone was established based on measurements for groundwater wells, engineering drawings for the CAS embankment (see the *Embankment Modeling* white paper), and consideration of the accuracy of the elevation measurements. The four wells are selected from a map of wells (Figure 7 in Bingham Environmental, 1991): GW-19A, GW-25, GW-27, and GW-60 as shown in Figure 2, since the location of these four wells bound the Class A waste cell. Each groundwater well is in the vicinity of one of the four corners of the CAS cell, so their measurements are treated as approximations to the water table elevation at the four corners. These water table elevations are also used to establish the distributions for the thickness of the saturated zone, and are documented in the *Saturated Zone Modeling* white paper.

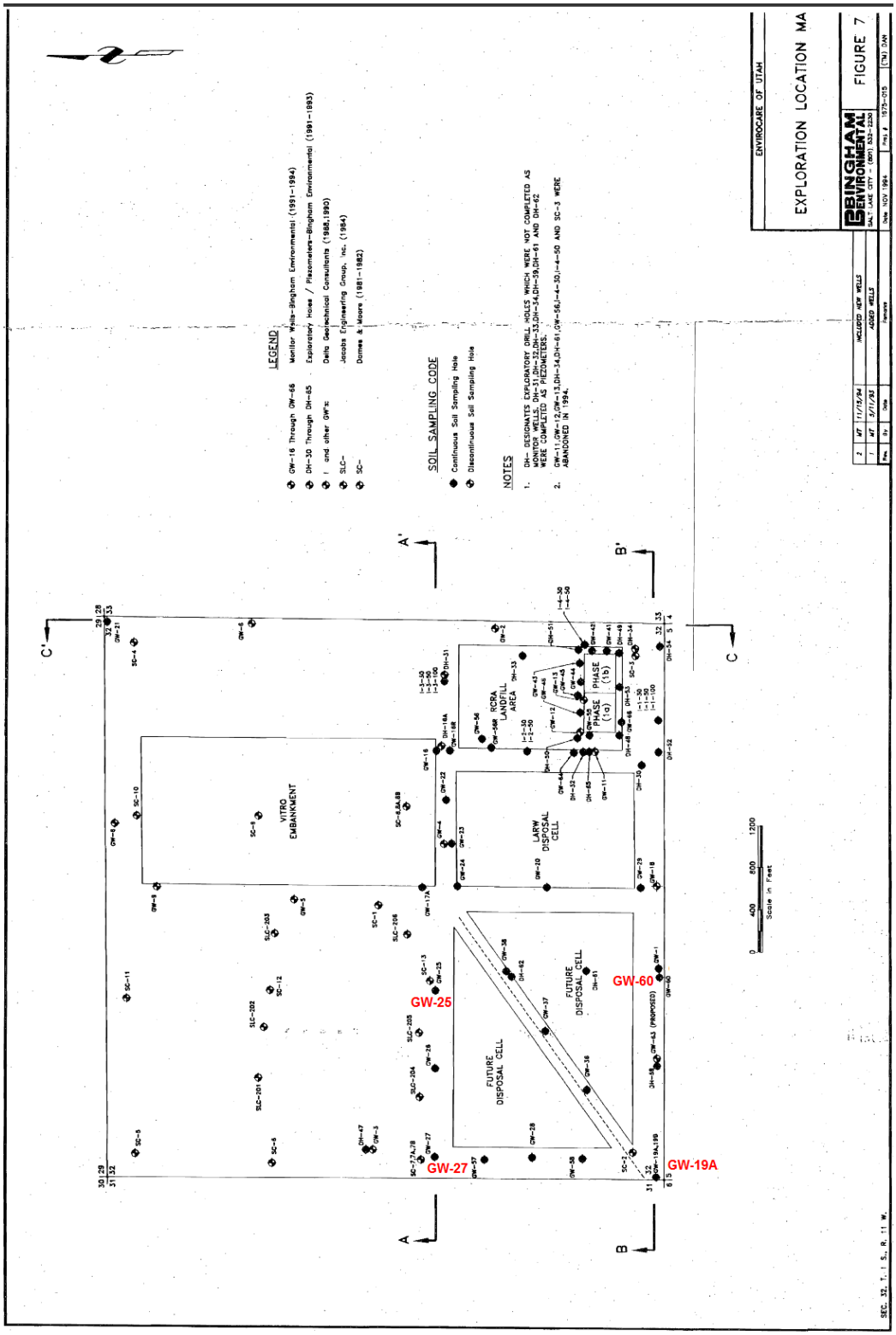

Figure 2. Locations of wells GW-1, GW-25, GW-27, and GW-19 (Figure 7 from Bingham Environmental, 1991)

In order to establish unsaturated zone thickness, the elevations for the water table are subtracted from the elevations for the bottom of the clay liner (see the *Embankment Modeling* white paper). The elevations of the bottom of the clay liner are interpolated for each of the four corners of the CAS cell to compute an unsaturated zone thickness for each corner. Based on the accuracy of the water table elevation measurements and the approximations involved in computing thicknesses, the calculated thickness for each corner was deemed to have measurement and reporting error with a standard deviation of 15 cm (0.5 ft). Since the average elevation across the cell is computed as the average elevation of the four corners, the standard error of the mean is 15 cm (0.5 ft) divided by the square root of 4. The resulting distribution for the mean thickness of the unsaturated zone was thus chosen as a normal distribution with mean equal to 3.93 m (12.9 ft) and a standard deviation of 7.6 cm (0.25 ft).

8.0 Numerical Solution for Unsaturated Flow

The computational method implemented in the Clive DU PA Model solves Equation 3 for steady state flow at constant infiltration flux, q. (At steady state, the vertical infiltration flux must be constant in all layers of the cell below the radon barriers, which includes the waste, the clay liner, and the Unsat zone.) No iterations are required with the selected solution technique. The approach in the Clive DU PA Model differs from the solution technique in the UNSAT-H code, which solves the transient (unsteady) equation for one-dimensional unsaturated flow and iterates to a steady state solution with constant infiltration rate.

8.1 Solution of the Darcy Equation by the Runge-Kutta Method

Equation 3 is a nonlinear, first order differential equation for the suction head that can be solved by numerical approximation. The Runge-Kutta method is attractive for this application because it allows variable spacing (i.e., variable Δz) between nodes, because it is highly stable, and because it does not require iteration to converge to a solution. Equation 3 can be rewritten as a first order differential equation in the form $h' = f(h)$:

$$\frac{\partial h}{\partial z} = \frac{q}{K_L(h)} - 1 \tag{32}$$

A second order Runge-Kutta solution for this first order differential equation is given by Abramowitz and Stegun (1970, Section 25.5.6):

$$h_{n+1} = h_n + \frac{k_1 + k_2}{2} + O(h^3), \tag{33}$$

with

$$k_1 = \Delta z \left(\frac{q}{K_L(h_n)} - 1 \right) \tag{34}$$

$$k_2 = \Delta z \left(\frac{q}{K_L(h_n + k_1)} - 1 \right) \tag{35}$$

and

$$\Delta z = z_{n+1} - z_{n.} \tag{36}$$

Equations 33 through 36 define a procedure for calculating h_{n+1} from the known values of h_n, Δz, and the (constant) infiltration flux, q. These equations constitute a predictor-corrector calculation, where k_1 is the predictor and k_2 is the corrector. No iteration is involved in this solution because Equations 34, 35, and 33 can be solved sequentially for each node of the grid, beginning with the lowest node at the top of the water table with $h = 0$ (because the suction head is zero for a saturated soil) and $K_L = K_s$, and integrating upward through the various unsaturated soil layers. Stable solutions do require a finer discretization than the layers that are defined for the 1-D columns used in the Clive PA model.

The value of Δz does not have to be constant over the domain of integration, and has been adjusted to provide reasonable accuracy where the head gradient is greatest. In practice, these regions occur at the capillary fringe just above the water table and at the interface between the clay liner and waste. The value of Δz has to be small enough that the predictor step (Equation 34) does not generate a value of k_1 that is so large and negative that $(h_n + k_1)$ becomes negative. Suction head is always positive, and $K_L(h_n + k_1)$ in Equation 35 cannot be evaluated for negative values of $(h_n + k_1)$. In practice, an initial node spacing of 2 cm provides a stable solution in Unit 3, directly above the water table, for the infiltration fluxes of interest. However, an initial node spacing of 0.1 mm was required to provide a stable solution in the waste, directly above the clay liner, at high infiltration rates. This fine spacing is required because the head gradient at the interface between the waste and clay liner is quite large. A node spacing of 25 cm provides a stable solution in the main body of the waste and in Unit 3 where the head gradients are smaller. A constant node spacing of 15 cm provides adequate resolution in the clay liner and in the upper and lower radon barrier. Solutions at these variable grid spacings are mapped to the Clive DU PA Model's regular grid that is used to represent wastes and other layers, in the top slope and side slope columns.

8.2 Verification of the Runge-Kutta Method

The UNSAT-H modeling program (Fayer 2000) has been used to analyze infiltration through the CAS cell at the Energy*Solutions* facility (Whetstone 2007). A model built with UNSAT-H predicted moisture content and suction head from the radon barriers in the cover downward through the waste, clay liner, and Unit 3 silty sand to the top of the aquifer (Whetstone 2007, Section 4 and Table 17). The results from the UNSAT-H calculation for the top and side slope models have been used to verify the steady state unsaturated flow solutions with the Runge-Kutta method outlined in Section 8.1.

The UNSAT-H calculations are based on a van Genuchten representation for soil moisture content and for soil hydraulic conductivity. For verification purposes, the Runge-Kutta solution was programmed into a spreadsheet using the identical van Genuchten models as UNSAT-H. The Runge-Kutta verification used the same total thicknesses for the radon barriers, waste, clay liner, and Unit 3 sand as the UNSAT-H model, but the spacing of individual nodes (i.e., the values of Δz) is different. Table 14 summarizes the thicknesses of the major components.

Table 14. Layer thicknesses and coordinates for top slope validation calculations.

Layer	Thickness	z-Coordinate
Upper Radon Barrier	1 ft (30.48 cm)	0 to 30.48 cm
Lower Radon Barrier	1 ft (30.45 cm)	30.48 cm to 60.96 cm
Waste	45 ft (1371.6 cm)	60.96 cm to 1432.56 cm
Clay Liner	2 ft (60.96 cm)	1432.56 cm to 1493.52 cm
Unit 3 Silty Sand	10.8 ft (329.2 cm)	1493.52 cm to 1822.7 cm

Figure 3(a) compares the calculated values for moisture content from the UNSAT-H model (Whetstone 2007, Table 17) and from the Runge-Kutta solution for the top slope model with an infiltration rate of 0.276 cm/yr. Both solutions encompass the radon barriers, the waste, the clay liner beneath the waste, and Unit 3 from the bottom of the clay liner to the top of the water table. The results are essentially identical, providing validation for the Runge-Kutta method. Figure 3(b) provides a more detailed comparison of moisture content near the bottom and top of the clay liner, again demonstrating the close agreement between the UNSAT-H model and the Runge-Kutta method.

A similar comparison was also performed for the side slope model with an infiltration rate of 0.595 cm/yr. The side slope model is similar to the top slope model, except the average waste thickness is 5.64 m (18.5 ft) rather than 13.7 m (45 ft). Figures 4(a) and 4(b) again demonstrate the close agreement between the UNSAT-H model and the Runge-Kutta method.

The calculated values for suction head from the UNSAT-H model and from the Runge-Kutta method were also compared for the top and side slope models. The suction head profiles in the radon barriers, waste, clay liner and Unit 3 are shown in Figure 5 for the top and side slope models. A qualitative comparison between the Runge-Kutta solution and the UNSAT-H results was performed because the UNSAT-H data for suction head were not tabulated, only presented graphically (Whetstone 2007, Figures 8 and 9). The comparison of suction heads from both methods again demonstrates that the Runge-Kutta solution is in excellent agreement with the results from the UNSAT-H model.

The results in Figures 3 and 4 highlight three important features of the response of the CAS cell to infiltration. First, the clay liner has a moisture content of about 0.42 (see Figures 3(b) and 4(b)) in the top and side slope models. This value is just below θ_s, which is 0.432 for the van Genuchten model. The radon barriers have slightly higher moisture contents, approximately 0.425 to 0.43 (see left-hand side of Figures 3(a) and 4(a)), again just below the saturated moisture content of 0.432. These results confirm that the clay liner and radon barriers remain very close to saturation for either model (top or side slope) and for two different infiltration rates (0.276 cm/yr or 0.595 cm/yr) in the CAS cell. Second, the waste drains to a relatively low moisture content, on the order of 0.06 for either slope model and infiltration rate. This behavior is consistent with the low moisture retention of a sandy material. Finally, suction head shows greater differences than moisture content for the top and side slope models. The suction head is more directly dependent

on flow rate (see Equation 32) than moisture content, and the factor of two difference in the flow rates for the top and side slope models is the probable cause of the differences in Figure 5(a) and 5(b).

8.3 Clive PA Model of the CAS Cell

The Runge-Kutta method has been incorporated into the Clive PA model for infiltration through the radon barriers, waste, clay liner and Unit 3 of the CAS cell at the Energy*Solutions* facility. The PA model of the CAS cell has a number of differences with the verification calculations discussed in the previous section. The major differences are as follows:

1. The moisture retention and hydraulic conductivity of the radon barriers and clay liner are defined by a Brooks-Corey/Mualem model that is based on the test data from CSU for Unit 4 cores GW17A-B2 and GW19A-B1.

2. The moisture retention and hydraulic conductivity of the Unit 3 silty sand between the clay liner and water table are defined by a Brooks-Corey/Mualem model that is based on the test data from CSU for Unit 3 cores GW18-B4 and GW17A-B5.

Integration of the Darcy equation from node n, with a known value of the suction head, h_n, and a known value of $\Delta z_n = z_{i+1} - z_n$, to node n+1 is based on the following sequential steps:

1. Calculate the moisture content, θ_n, corresponding to the suction head, h_n. The calculation of θ_n is based on Equations 4 and 6 in Section 4.4.

2. Calculate the conductivity, $K(h_n)$, based on the effective saturation, Θ_n, at θ_n. Equations 6 and 9 in Section 4.4 define the formulas.

3. Calculate $k_1 = \Delta z_n(q/K(h_n) - 1)$ (see Equations 34 and 36 in Section 8.1).

4. Calculate the trial value of the suction head, $h_n + k_1$.

5. Calculate the trial value of the moisture content, $\theta(h_n + k_1)$ using Equations 4 and 6 found in Section 4.4.

6. Calculate the trial value of the conductivity, $K(h_n + k_1)$, based on the effective saturation at $\theta(h_n + k_1)$. Equations 6 and 9 in Section 4.4 define the formulas.

7. Calculate $k_2 = \Delta z_n(q/K(h_n + k_1) - 1)$ (see Equations 35 and 36 in Section 8.1).

8. Calculate $h_{n+1} = h_n + (k_1 + k_2)/2$ (see Equation 33 in Section 8.1)

Numerical testing demonstrated that the trial value of the suction head, $h_n + k_1$, can become negative, leading to an undefined value for $K(h_n + k_1)$. Negative values of $K(h_n + k_1)$ occurred at the interface between the waste and clay liner when the infiltration rate increased from 0.3 to 0.5 cm/yr for the as-designed cover to approximately 5 cm/yr. The numerical problem appears in the waste, adjacent to its interface with the clay liner, because the gradient of suction head is greatest at this location (for example, see Figure 5(a) at a depth of about 1,400 cm).

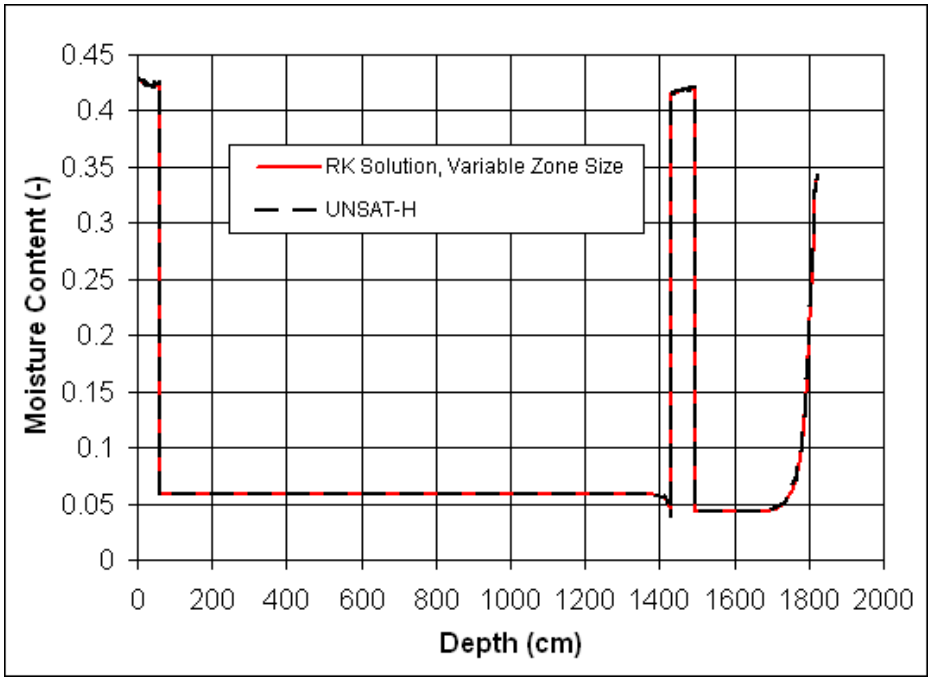

(a) Comparison of moisture content in Unit 3, clay liner, waste, and radon barriers

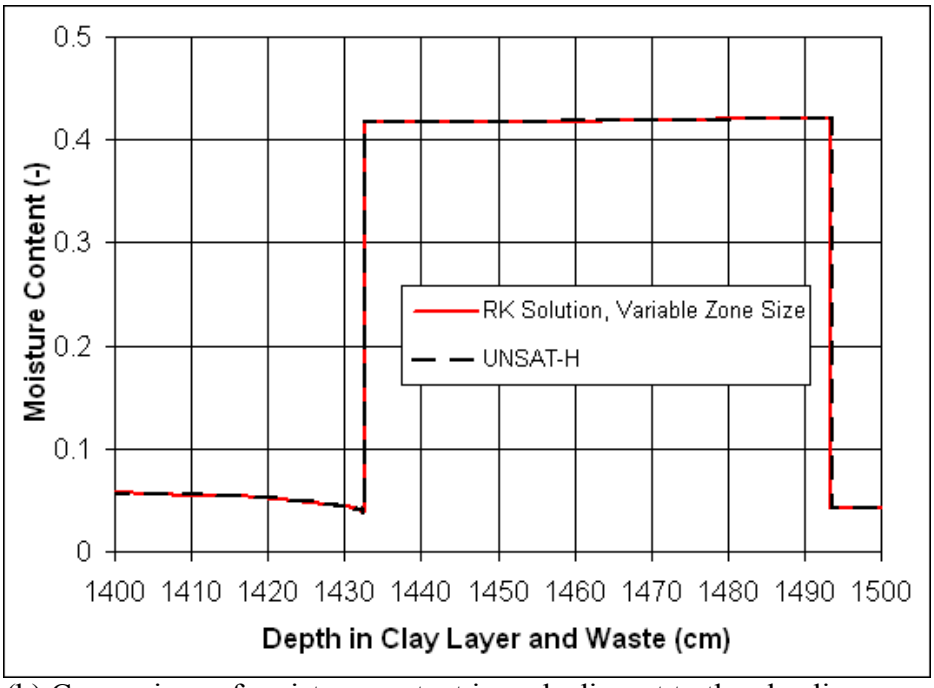

(b) Comparison of moisture content in and adjacent to the clay liner

Figure 3. Comparison of the Runge-Kutta and UNSAT-H solutions for top slope model.

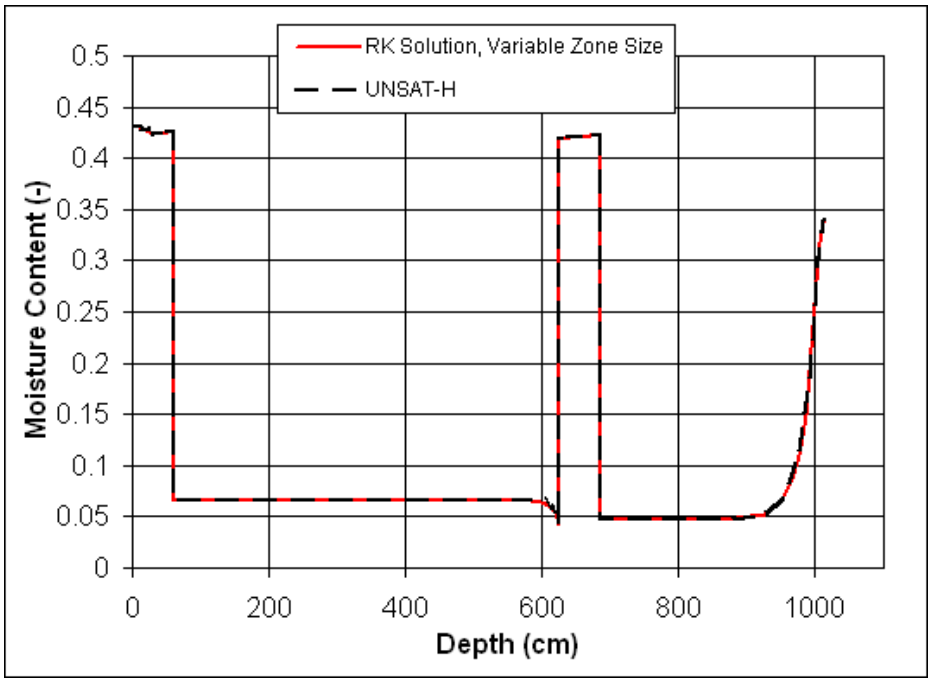

(a) Comparison of moisture content in Unit 3, clay liner, waste, and radon barriers

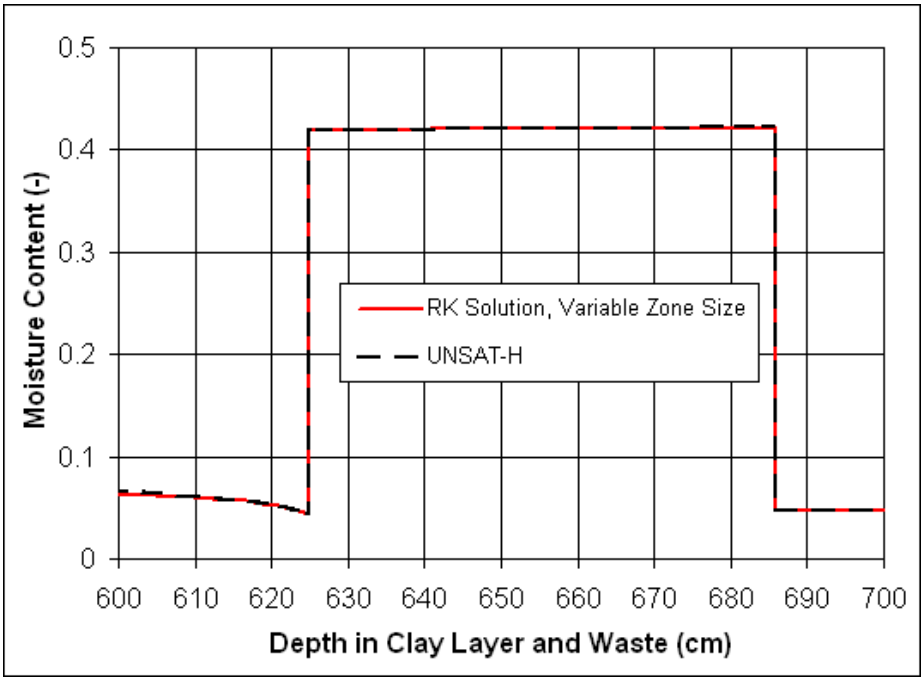

(b) Comparison of moisture content in and adjacent to the clay liner

Figure 4. Comparison of the Runge-Kutta and UNSAT-H solutions for side slope model.

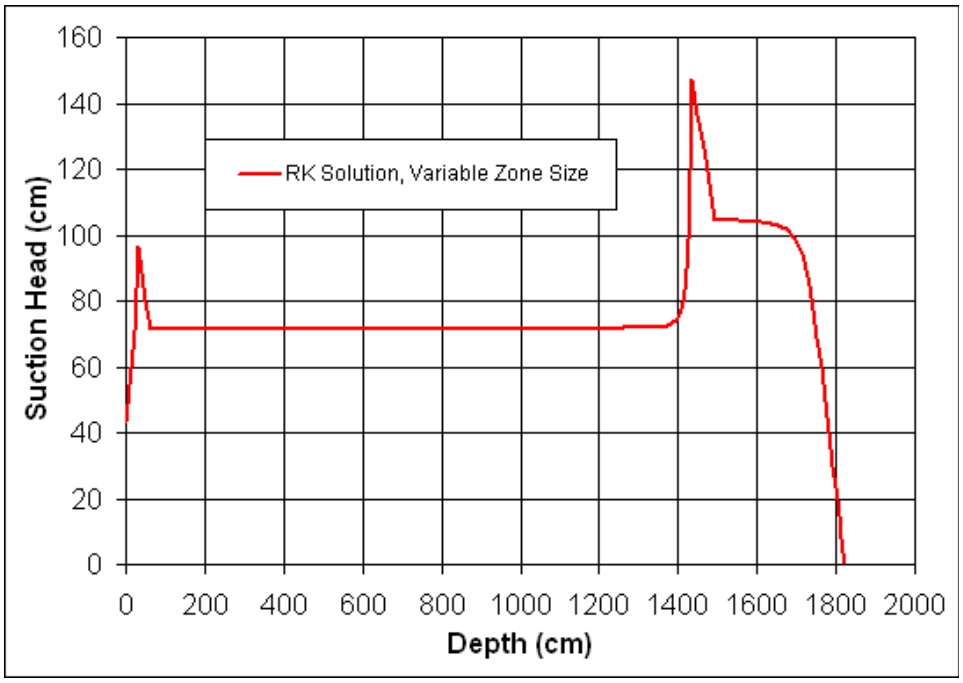

(a) Top Slope Model

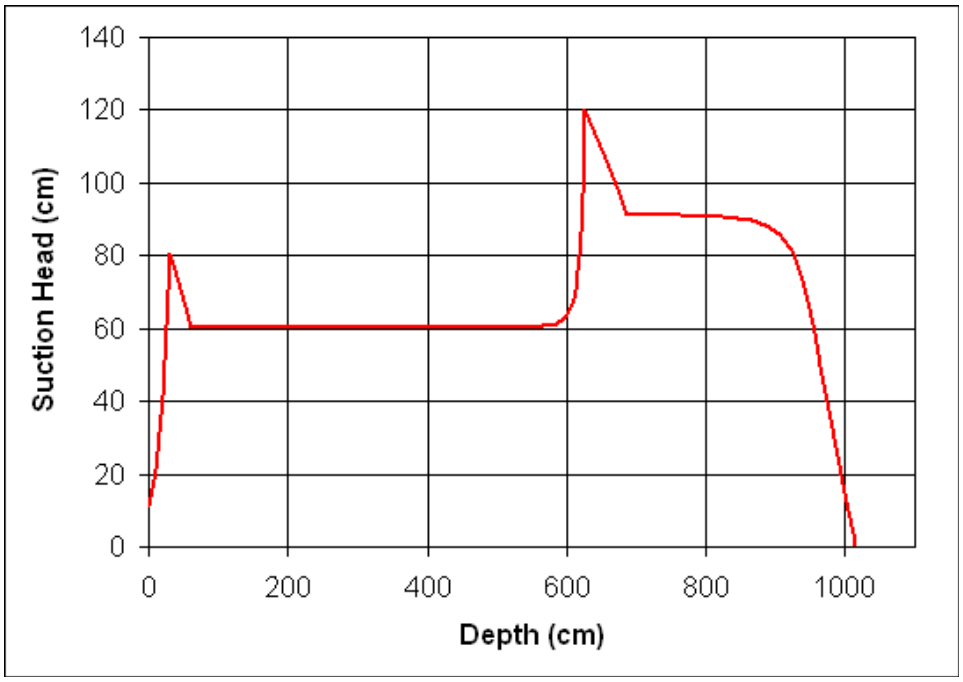

(b) Side Slope Model

Figure 5. Suction head profiles in Unit 3, clay liner, waste, and radon barriers for the top slope and side slope models.

The verification testing in Section 8.2 used the following spacing for nodes in the waste, adjacent to the clay liner: (1) 2-cm node spacing for the first five nodes in the waste, (2) 5-cm node spacing for the next 4 nodes in the waste, and (3) 25-cm node spacing for all other nodes in the waste. The GoldSim implementation of this solution uses a geometric spacing between the first 12 nodes in the waste, beginning with an initial spacing of 0.1 mm, which increases by a ratio of approximately 1.93 for each subsequent node. The spacing between the 11^{th} and 12^{th} nodes is 0.135 m and the total width of the 12 nodes with geometric zoning is 0.281 m. All subsequent nodes in the waste have a constant spacing of 0.281 m in the GoldSim implementation. Numerical testing demonstrated that the geometric zoning produces stable solutions for the top slope and side slope models with the Runge-Kutta method up to flow rates of 5 cm/year.

8.4 Numerical Testing of the Top Slope Model in GoldSim

Validation of a top slope infiltration model for the CAS cell was performed in GoldSim, using the same Runge-Kutta method and the same descriptions of soil properties, providing a direct comparison of results and a means of identifying errors in programming. Deterministic calculations were performed with Brooks-Corey/Mualem models for the individual cores (Unit 4 core GW17A-B2 or GW19A-B1, and Unit 3 core GW17A-B5 or GW18-B4) to compare unsaturated flow conditions calculated using GoldSim. Stochastic calculations were performed with GoldSim for 20 realizations using randomly sampled values for the Brooks-Corey/Mualem input parameters for Units 3 and 4. The GoldSim results for Realization 18 were identical to a calculation for Realization 18 to 5 or 6 significant digits. This testing also provided useful insights into the range of conditions in the CAS cell during unsaturated flow.

Figures 6 and 7 compare the profiles for moisture content and suction head, respectively, in the radon barriers, waste, clay liner, and Unit 3 for the four deterministic calculations that use Unit 3 (silty sand) properties for GW18-B4 or GW17A-B5 and use Unit 4 (silty clay) properties for GW17A-B2 or GW19A-B1. All calculations have an infiltration rate of 0.276 cm/yr (0.109 in/yr). These results confirm previous observations: (1) The moisture contents of the clay liner and radon barriers remain close to saturation, and (2) the waste retains a low moisture content of 0.06. In addition, the suction heads in the radon barriers are identical because the hydraulic conductivity is identical for either core (because conductivity was only measured for one of the two cores).

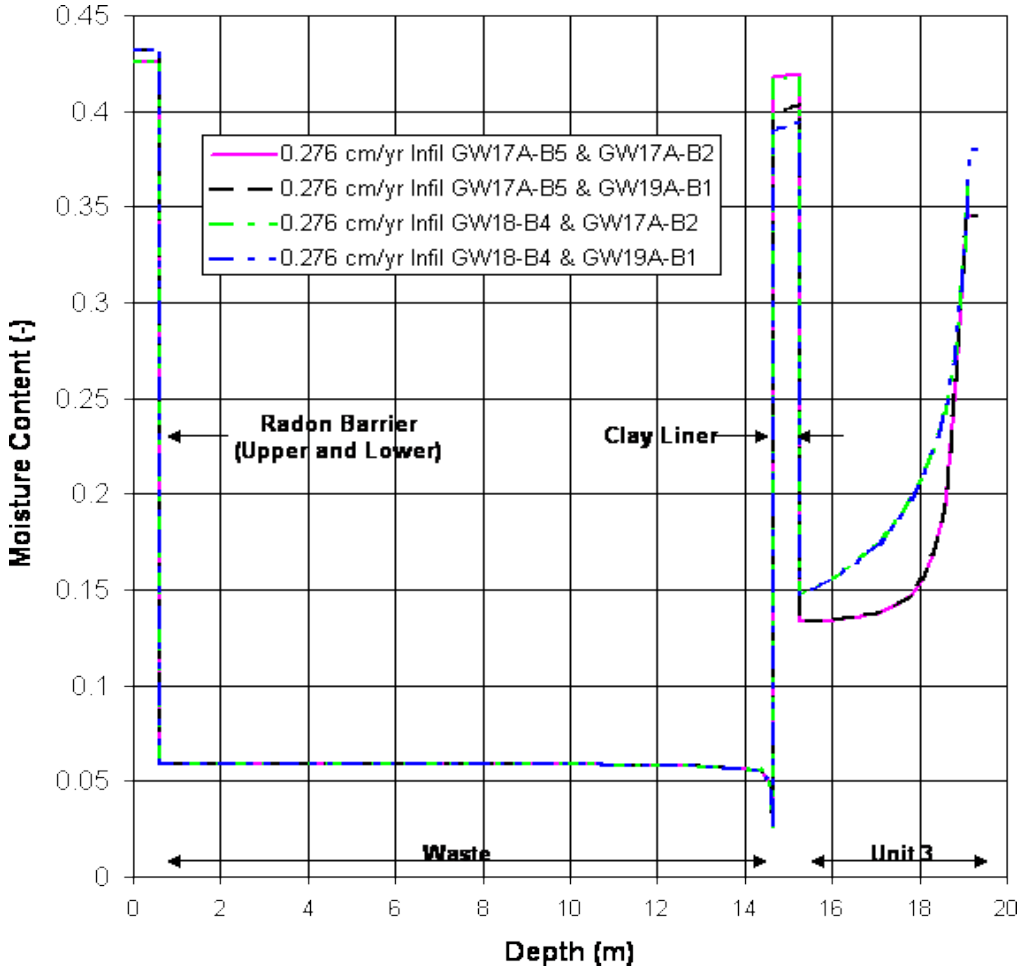

Figure 6. Profiles of moisture content in Unit 3, clay liner, waste, and radon barriers for the top slope model with 0.276 cm/yr infiltration.

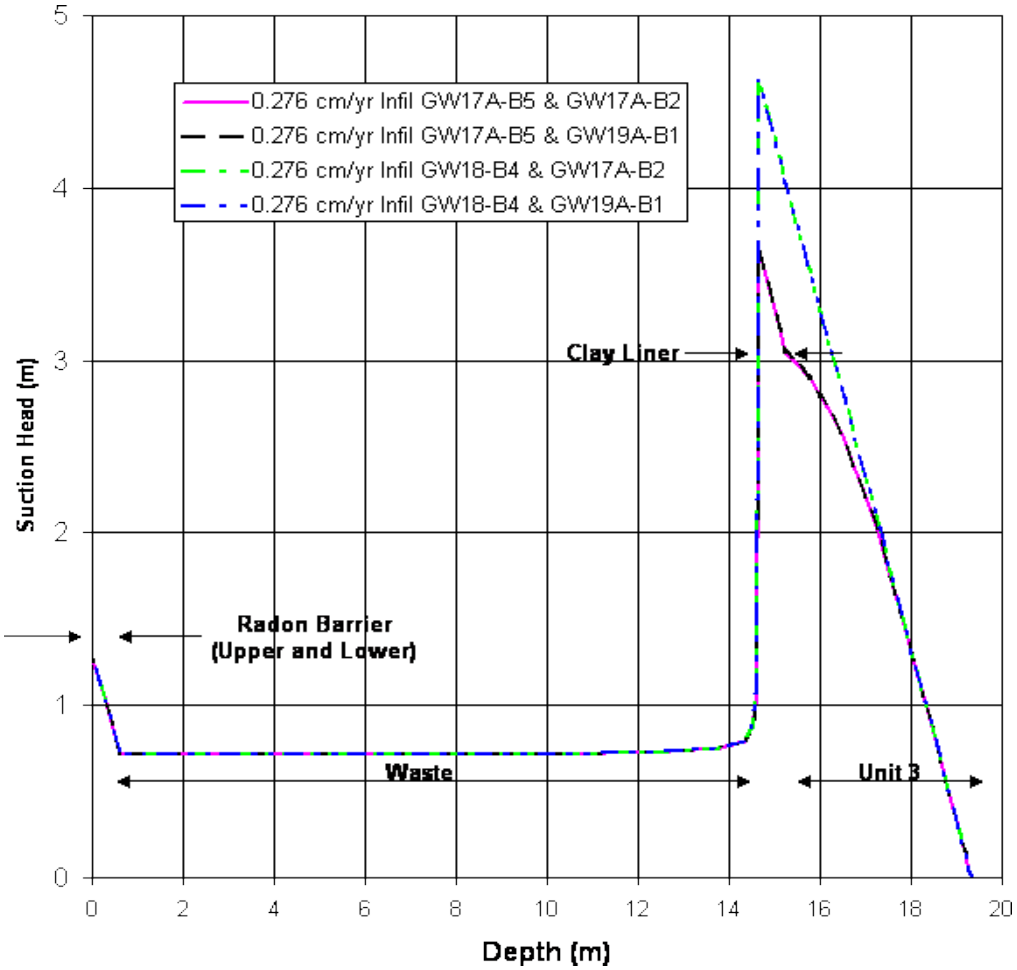

Figure 7. Profiles of suction head in Unit 3, clay liner, waste, and radon barriers for the top slope model with 0.276 cm/yr infiltration.

Figures 8 and 9 compare the profiles for moisture content and suction head, respectively, in the radon barriers, waste, clay liner, and Unit 3 for deterministic calculations that use soil properties for GW17A-B5 (Unit 3) and GW17A-B2 (Unit 4) at three different infiltration rates: 0.168 cm/year, 0.276 cm/yr, and 5.0 cm/yr. In general, Figures 8 and 9 demonstrate that moisture content is more sensitive to infiltration rate than to the differences between soil properties for the various cores. The major difference in Figure 8 is the degree of drainage in the waste, with the high infiltration rate increasing the retained moisture from 0.055 at 0.168 cm/yr to 0.084 at 5.0 cm/yr infiltration. The moisture content in the waste also shows a small oscillation between 0.082 to 0.086 at the 5.0-cm/yr infiltration rate. This could have be eliminated by having finer spacing between the nodes in the waste, but the accuracy of the current solution is considered more than adequate.

Similar calculations were also performed for soil properties with GW17A-B5 for Unit 3 and GW19A-B1 for Unit 4. The results are very similar to those shown in Figures 8 and 9 and are not repeated here.

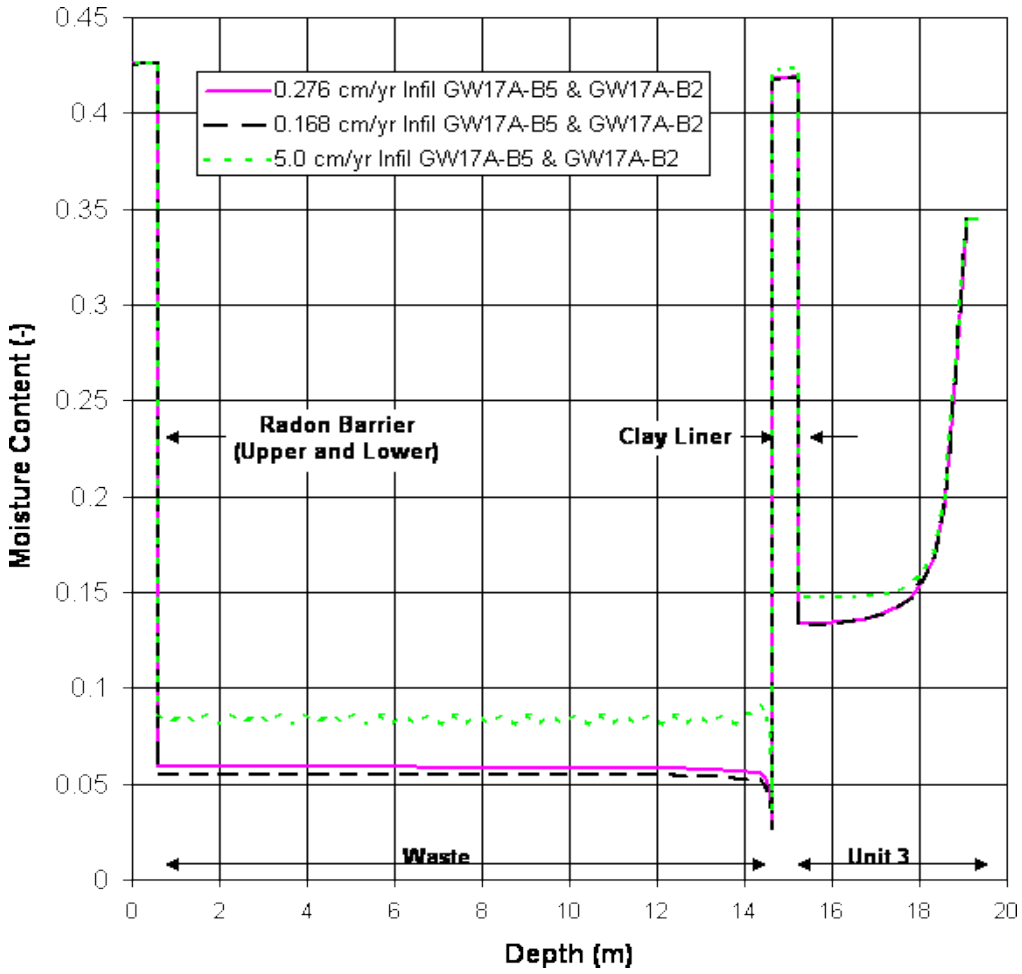

Figure 8. Profiles of moisture content in Unit 3, clay liner, waste, and radon barriers for the top slope model with different infiltration rates.

Figures 10 through 14 compare the time dependent moisture content at the mid-points of Unit 3, of the clay liner, of the waste, of the lower radon barrier, and of the upper radon barrier, respectively, for a GoldSim calculation with 20 realizations and randomly sampled soil properties for Units 3 and 4. The duration of each realization is 3,000 years and the lower filter layer is assumed to become degraded at 2,640 years after closure for test purposes.

The results in Figures 10 through 14 confirm the observations from the previous calculations: (1) the moisture contents in the clay liner, lower radon barrier, and upper radon barrier remain close to saturation (note the expanded vertical scale for Figures 13 and 14), and (2) the waste drains to low moisture content, 0.03 to 0.08, for these 20 realizations, and (3) the moisture content in Unit 3 also has a limited range of 0.13 to 0.20 for the infiltration rates generated by the cover infiltration model.

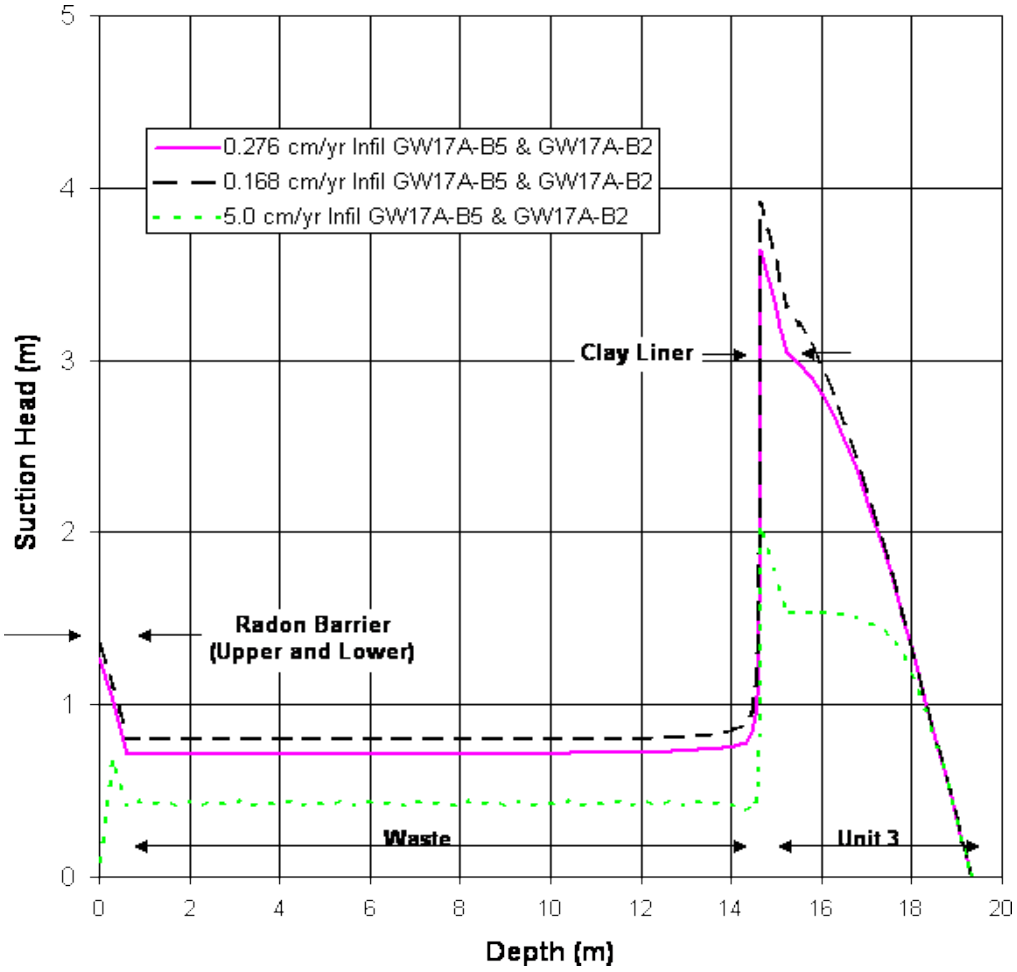

Figure 9. Profiles of suction head in Unit 3, clay liner, waste, and radon barriers for the top slope model with different infiltration rates.

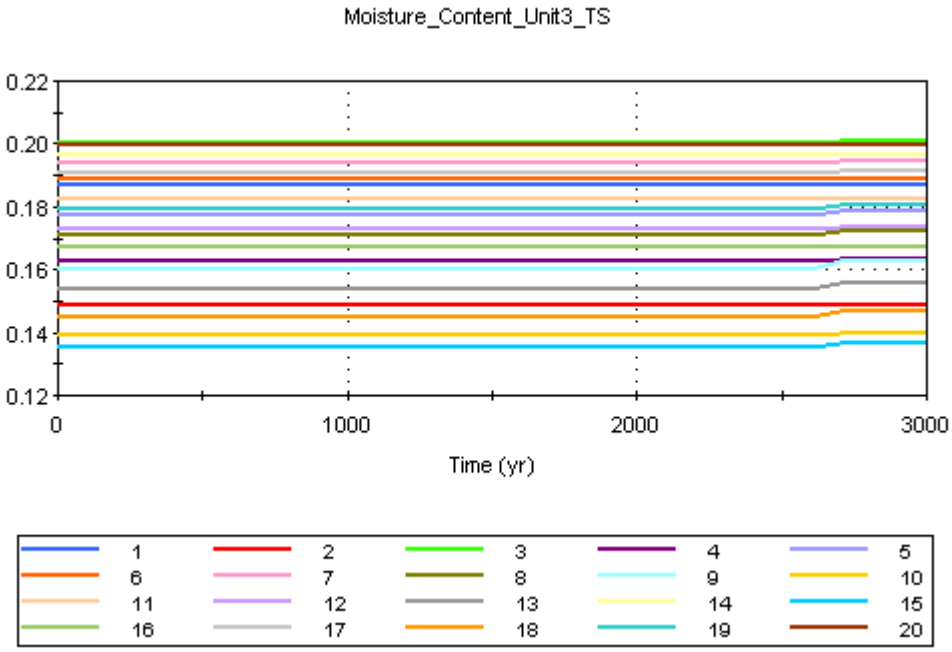

Figure 10. Time dependent moisture content from 20 realizations at the mid-height of Unit 3 with sampled soil properties for Units 3 and Unit 4.

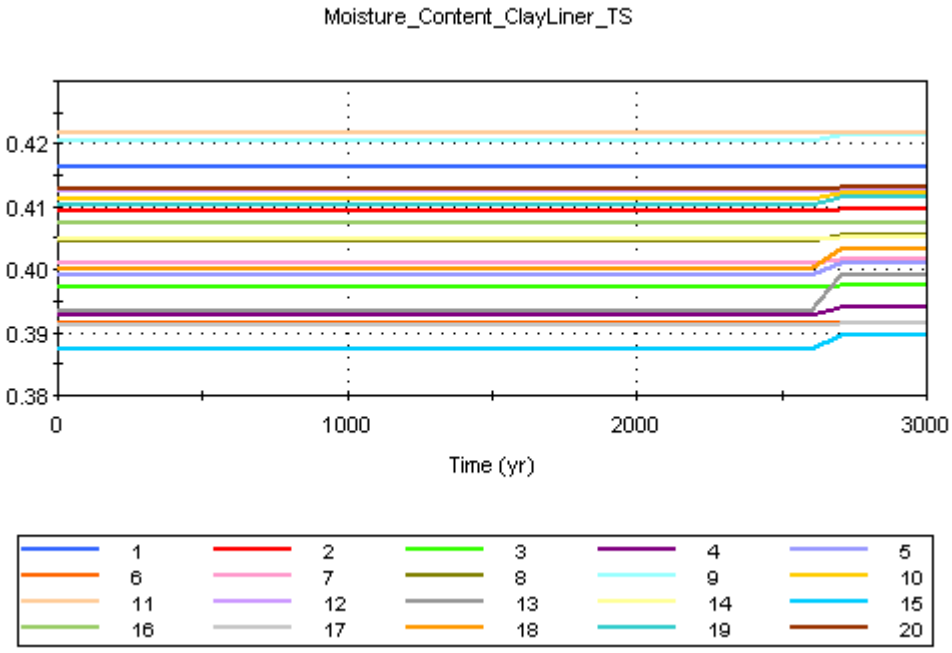

Figure 11. Time dependent moisture content from 20 realizations at the mid-height of the clay liner with sampled soil properties for Units 3 and Unit 4.

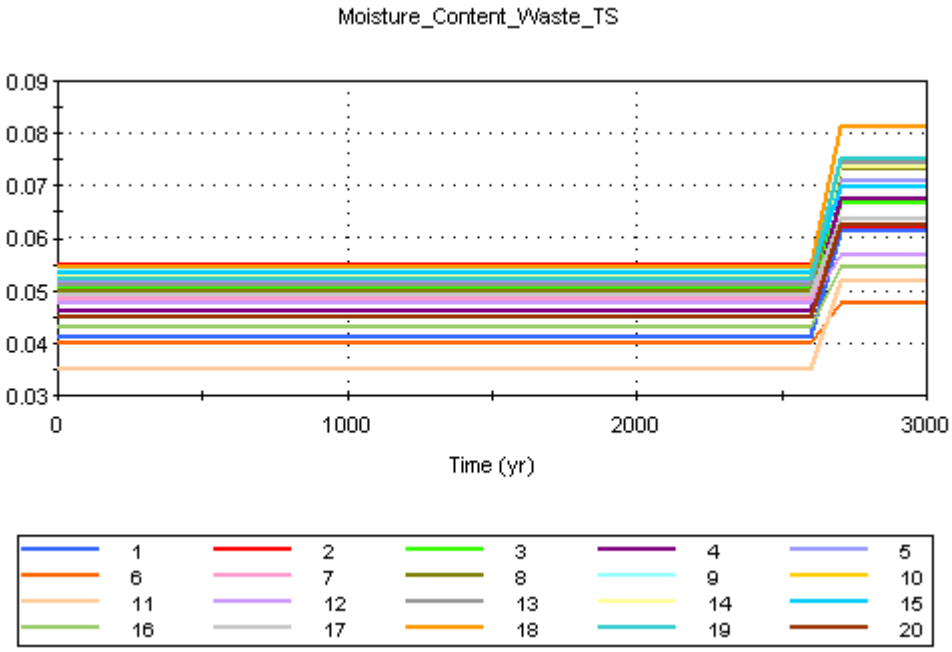

Figure 12. Time dependent moisture content from 20 realizations at the mid-height of the waste with sampled soil properties for Units 3 and Unit 4.

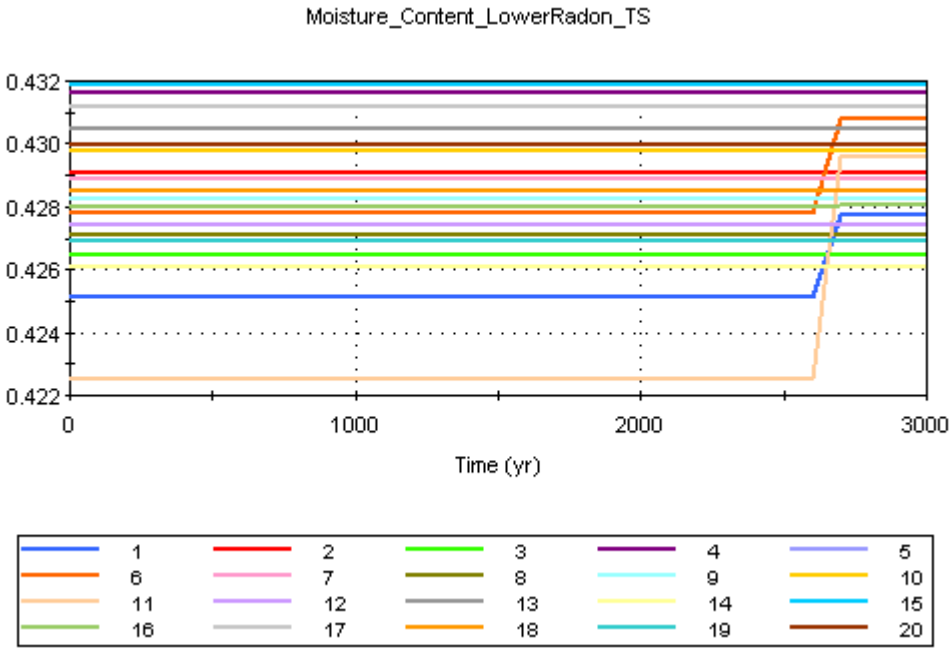

Figure 13. Time dependent moisture content from 20 realizations at the mid-height of the lower radon barrier with sampled soil properties for Units 3 and Unit 4.

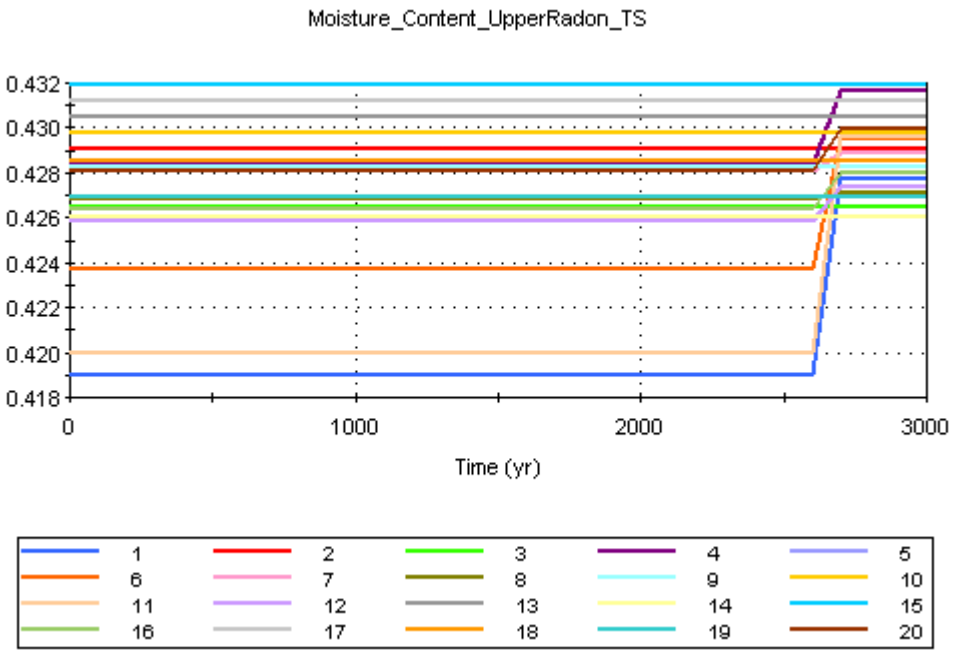

Figure 14. Time dependent moisture content from 20 realizations at the mid-height of the upper radon barrier with sampled soil properties for Units 3 and Unit 4.

9.0 Contaminant Fate and Transport in Porous Media

Once all the hydraulic properties and states have been developed, as in the previous sections, we can turn to transport mechanisms within the various porous media. Contaminant transport takes place in fluid phases—in the present case, this is limited to air and water. Fluids move through the pores by advection in response to fluid pressure gradients, carrying dissolved contaminants with them. Fluids are also a medium for diffusive transport, in which contaminants move simply in response to concentration gradients, and do not require movement of the fluid. Both these processes occur simultaneously, along with all the other mechanisms identified in the model for contaminant transport (radioactive decay and ingrowth, geochemical partitioning, biotically-induced transport, erosion, etc.) This section discusses advective and diffusive contaminant transport mechanisms in fluids.

9.1 Porous Medium Water Transport

Water is a significant transport mechanism at Clive, and the conceptual model is that water slowly percolates down from the ground surface to the water table, and that diffusion can occur in the water phase as well.

9.1.1 Advection of Water

The flow of water is discussed at length in the previous sections of this document. Contaminant transport in this flowing water is essentially passive, with solutes moving along with the fluid, though of course concentrations are affected by other simultaneous processes.

9.1.2 Diffusion in Water

The Clive DU PA Model employs a modified version of GoldSim's native diffusive flux links to calculate diffusive fluxes in porous media. The modifications are necessary to account for unsaturated media, since GoldSim assumes that porous media are saturated in its basic implementation of diffusive flux calculations. The standard GoldSim diffusive flux mathematics are covered in Appendix B of the GoldSim User's Guide (GTG, 2011), and the modifications that have been developed by Neptune are discussed in detail in the Neptune document entitled *Modeling Diffusion in GoldSim*, but are also covered briefly here. The modifications required to model diffusion in unsaturated media take two phenomena into consideration: 1) The diffusive area is reduced by the saturation (with respect to air or water, whichever medium is of interest) and 2) the diffusive length is increased to account for tortuosity in the respective medium.

If a porous medium contains only a single fluid phase, the diffusive area between two cells containing that medium is simply the total area times the porosity, since the pores are occupied by the fluid, and the diffusion takes place only in the fluid. In the case of two fluids, such as air and water in unsaturated media, the diffusive area is further reduced, since the area of the fluid of interest across the plane of diffusion is less. If we are interested in diffusion in the water phase, for example, the area of water that intersects the plane is equal to the total area times the water content, which equals the total area times the porosity times the saturation with respect to water. If we are interested in diffusion in the air phase, we use the same construct, substituting air for water. Because the diffusive area is always less, the diffusion in a unsaturated medium will always be less than that in a fully saturated medium.

Diffusion in unsaturated media is also attenuated because of increased tortuosity. In any porous medium, a diffusing solute must travel through pores, following a tortuous path that is always longer than if it were traveling in a straight line. The ratio of the straight line distance to this tortuous path is called the tortuosity. If the porous medium is unsaturated, this path becomes even longer, since the three dimensional shape of the fluid of interest gets even more tortuous. This increases the diffusive length, which is used in calculating the concentration gradient. The gradient in concentration of a solute is what drives diffusion.

9.1.3 Water phase Tortuosity

Tortuosity is a term used to describe the resistive and retarding influence of pore structure for a variety of transport processes (Clennell, 1997). Definitions of tortuosity are not consistent in the literature and depend on the discipline and the particular transport process of interest. The tortuosity τ for molecular diffusion in porous media can be written as the ratio of effective diffusivity D_{eff} to bulk diffusivity D_{bulk}, often seen in two forms:

$$\tau_1 = \frac{D_{eff}}{D_{bulk}} \tag{37}$$

or alternatively, if exclusion of the measured porosity n is desired (Clennell, 1997), as

$$\tau_1 = \frac{D_{eff}}{n D_{bulk}}. \tag{38}$$

In this definition, consistent with the assumptions of GoldSim, the value of tortuosity varies between 0 and 1, with lower values indicating a longer path for porous medium solute transport via advection or diffusion. For unsaturated systems n is replaced in equation (38) by water content θ_w for water phase diffusion, or by the volumetric air content θ_a, for gaseous phase diffusion. The form shown in equation (37) is found in Freeze and Cherry (1979) and Marsily (1986) while that in equation (38) is used by Hillel (1980) and Koorevaar et al. (1983).

For consistency with GoldSim the second form is used. The equations for diffusive conductance in GoldSim explicitly specify the effective porosity (or in the case of unsaturated flow, water content or air filled porosity) as in equation (38). For more information on the diffusion equations in GoldSim, see Appendix B of the GoldSim User's Guide (GTG 2011). In the following sections, the equations from the literature have been converted where necessary to be consistent with equation (38) so that they can be directly applied to PA models.

Two options were considered for modeling liquid phase tortuosity in the Models. The Millington-Quirk model is commonly used to estimate tortuosity in non-fractured porous media (Millington and Quirk, 1961) (see Jury and Horton, 2004, eq. 7.14, modified by division by water content for consistency with GoldSim.) The water phase tortuosity τ_w is calculated as

$$\tau_w = \frac{D_{eff}}{\theta_w D_{bulk}} = \frac{\theta_w^{7/3}}{n^2}. \tag{39}$$

An alternative estimate of tortuosity has been developed from an empirical relationship between D_{eff} and θ_w from measurements provided by Conca and Wright (1992). Effective diffusivities for over 300 samples were determined for NaCl and KCl solutions using their Unsaturated Flow Apparatus (UFA) to establish the water content and other physical conditions in the sample. The relationship between D_{eff} and θ_w for a range of soils and gravels is shown in Figure 15. The relationship is remarkably consistent over a wide range of materials, indicating that it is insensitive to the grain size of the porous medium.

The model is expressed as

$$\log_{10} D_{eff} = -4.1 + 2.7 \log_{10}(\theta_w) + 0.32 \log_{10}(\theta_w)^2. \tag{40}$$

Volumetric water content is expressed as a fraction and D_{eff} has implied units of cm^2/s. Using D_{bulk} of 2.03×10^{-5} cm^2/s for chloride (Domenico and Schwartz 1990, p. 369), water tortuosity can be estimated from equations (39) and (40) for all solutes:

$$\tau_w = \frac{D_{eff}}{\theta_w D_{bulk}} = \frac{10^{-4.1 + 2.7 \log_{10}\theta_w + 0.32 \log_{10}\theta_w^2}}{\theta_w \, 2.03 \times 10^{-5} \, cm^2/s}. \tag{41}$$

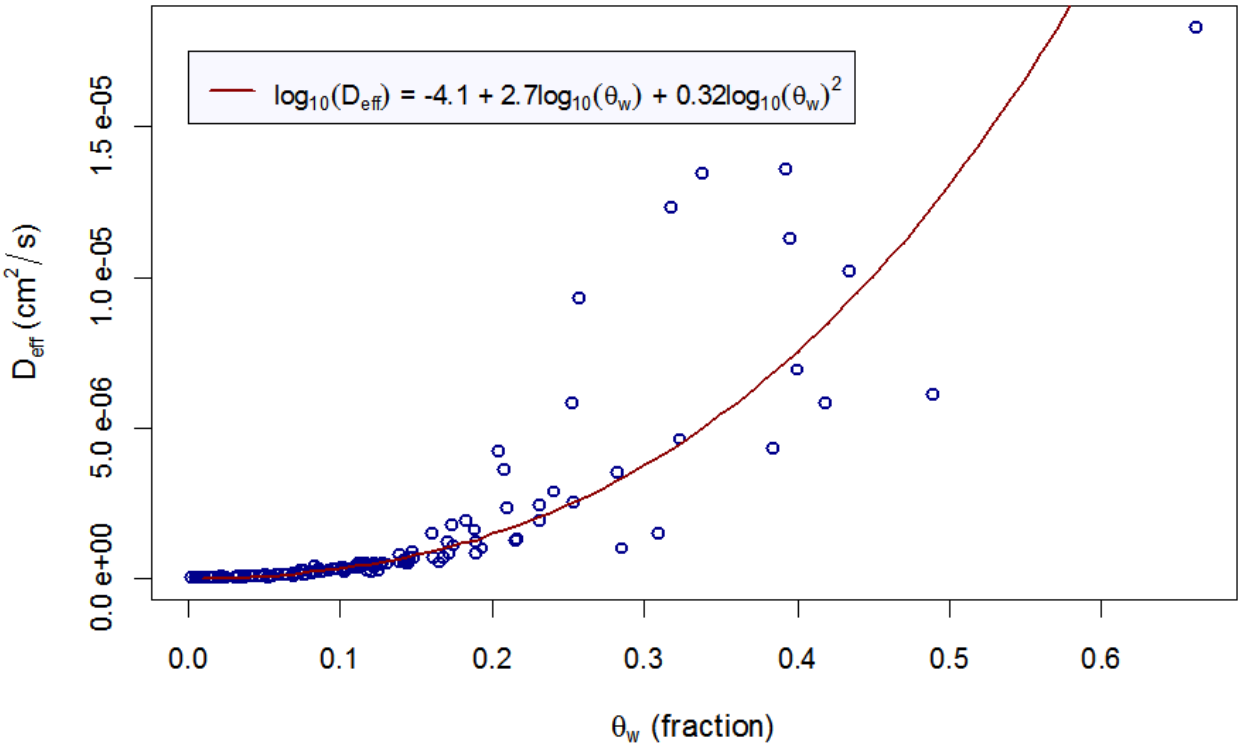

Figure 15. Estimated values of effective diffusivity D_{eff} for a range of volumetric water content for the Conca and Wright (1992) model. (After Conca and Wright, 1992).

The two tortuosity models are compared in Figure 16 using an effective porosity value of 0.37 for the Millington-Quirk model. Over the range of volumetric water contents from 0.10 to 0.20 the models differ by factors ranging from approximately 5 to 2.

Millington and Quirk (1961) concluded that, when considering porosity as the effective area of flow, the range on the porosity exponent in Equation (39) could be between 0.5 and 2 depending on the characteristics of the medium. This provided the foundation for developing input distributions for the exponents in porosity and water content in the Millington-Quirk model that model a range of behaviors that spanned the Millington-Quirk model and the Conca and Wright data. Generalizing the Millington-Quirk model gives:

$$\tau_w = \frac{D_{eff}}{\theta_w D_{bulk}} = \frac{\theta_w^{\beta_\theta}}{n^{\beta_n}} \tag{42}$$

where

β_θ is the water content exponent, and
β_n is the porosity exponent.

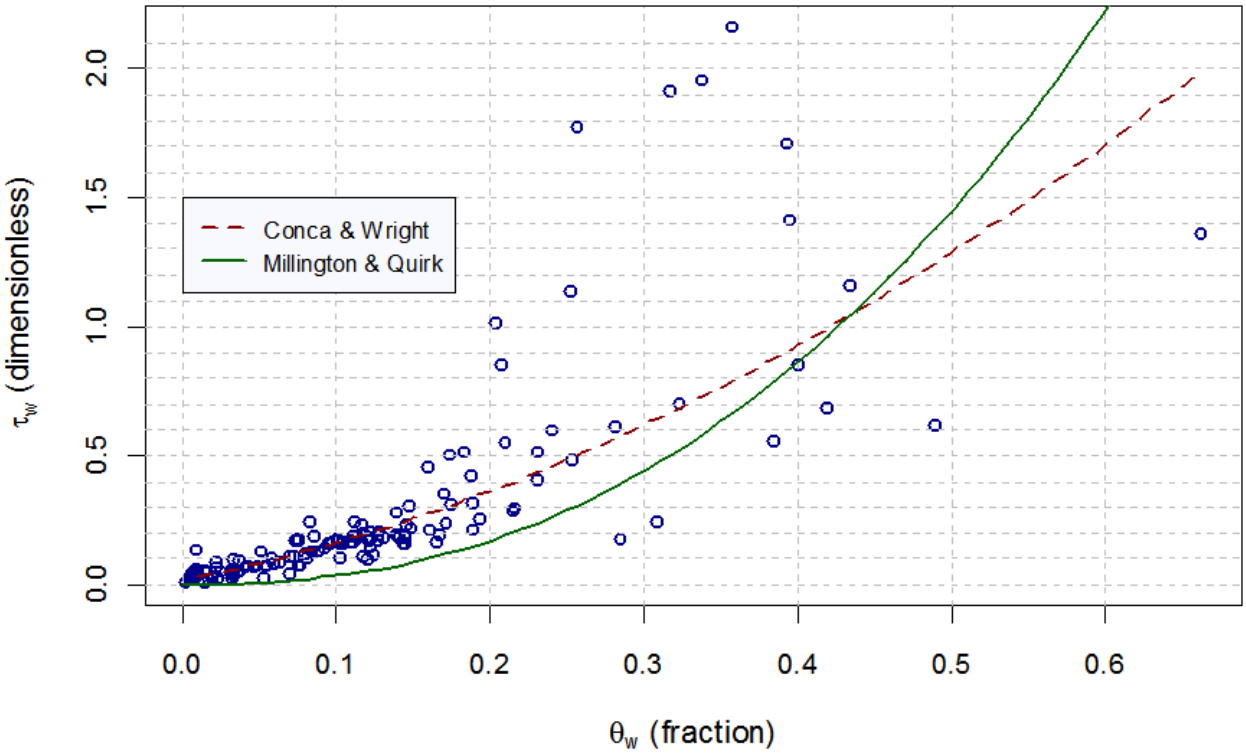

Figure 16. Water phase tortuosity function comparison between Millington-Quirk (Jin and Jury 1996) and Conca and Wright (1992).

Choosing a uniform distribution with a minimum of 0.5 and a maximum of 2.0 for β_n and a uniform distribution with a minimum of 4/3 and a maximum of 7/3 for β_θ results in the range of behaviors presented in Figure 17. These values are utilized in the Clive PA Model parameters to provide a conservatively high estimate of uncertainty, to allow the sensitivity analysis to determine the model is sensitive to the value of β_n. The upper bound on simulated tortuosity is given by $\beta_n = 2$ and $\beta_\theta = 4/3$ and the lower bound is given by $\beta_n = 1/2$ and $\beta_\theta = 7/3$. This appears to adequately describe a range of behaviors that includes the original Millington-Quirk model, the Conca and Wright data and a modeling analysis of unsaturated zone behavior in arid environments (Wolfsberg and Stauffer, 2003).

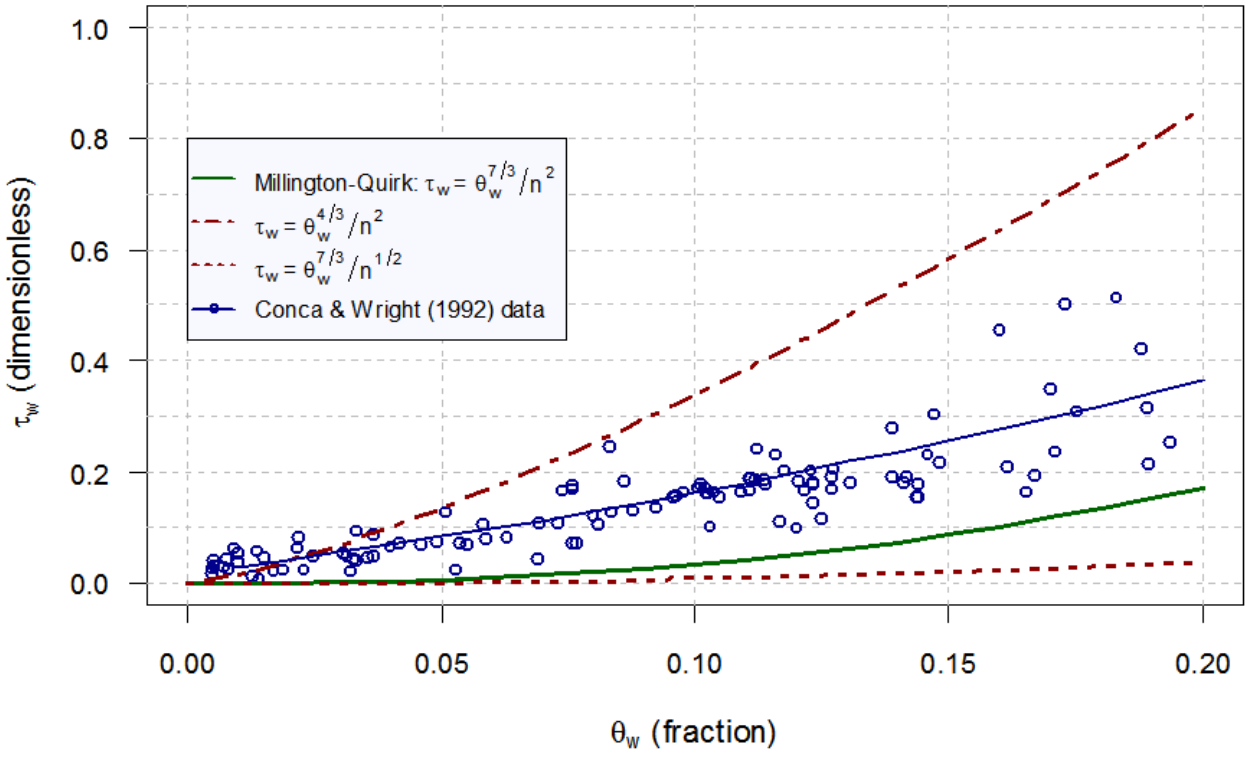

Figure 17. Comparison of the Millington-Quirk (1961) based water phase tortuosity formulation and the Conca and Wright model and data (1992).

9.2 Porous Medium Air Transport

9.2.1 Advection of Air

Air-phase advection is not included in the Clive DU PA Model. It is assumed that the advective flux of gases is negligible compared to the diffusive gas flux.

9.2.2 Diffusion in Air

Air-phase diffusion is included in the model, and this is the principal process by which gases are moved. The "built-in" diffusion calculations in GoldSim are used to estimate diffusion in the air phase. These gaseous diffusive fluxes are modified to handle the unsaturated porous media (described above in Section 9.1.2), but also include a calibration to counteract numerical dispersion for radon (discussed below in Section 9.4.2), which at this time is the only radionuclide that is considered to be present in the gaseous phase. The free-air diffusion coefficient for radon is fixed at 0.11 cm^2/s (Rogers and Nielson, 1991, p.226), since this is a well-established value with little uncertainty. Partitioning between the air and water phases is also handled internally by GoldSim, with the aid of the definition of Henry's Law constants for the various gas-phases constituents, discussed in Section 9.3.

Diffusion in the air phase is modeled throughout the top slope and side slope columns, bounded at the bottom by the saturated zone, and at the top by the atmosphere. The bottom boundary condition is one of no diffusion, since there is no air in the saturated zone to diffuse into, by definition. The boundary condition at the top is effectively a zero-concentration sink, since the volume of air in the atmosphere flowing over the embankment is sufficiently large that concentrations are kept much lower than in the pore air of the cover and wastes below. In order to model this, the air directly above the embankment is represented by an Atmosphere Cell Pathway element in GoldSim. The volume of air is defined by a thickness times the area of each respective modeled column, and this air volume is flushed out by the wind. The diffusive flux from the uppermost cover cell in the column to the Atmosphere cell is defined by the diffusive area, as discussed above, and the diffusive length, discussed in the following section. Since the atmosphere is not a porous medium, a diffusive length unrelated to its thickness is adopted. Since the wind will maintain low concentrations in the atmosphere, amounting to a zero-concentration boundary condition, the choice of the parameters defining the Atmosphere is not expected to have much influence on the diffusive flux from the embankment cover. Small uncertainties have been selected for these values, as shown in Table 15, in order to evaluate the model's sensitivity.

Table 15. Atmosphere volume parameters for creating a surface boundary condition in the porous medium air diffusion model.

Parameter	Distribution	Units
Thickness of the atmosphere layer	N(μ=2.0, σ=0.5, min=Small, max=Large)	m
Wind speed	N(μ=3.14, σ=0.5, min=Small, max=Large)	m/s
Atmospheric diffusion length	N(μ=0.1, σ=0.02, min=Small, max=Large)	m

9.2.3 Air-Phase Tortuosity

A number of tortuosity models have been proposed for air phase diffusion in porous media. Using the form for tortuosity shown in (38) above, models reviewed by Jin and Jury (1996) include the Penman model (Penman, 1940) and two models attributed to Millington and Quirk. In the Penman model, air phase tortuosity τ_a is a constant:

$$\tau_a = 0.66 . \tag{43}$$

In the more commonly used Millington-Quirk model (MQ1), which is analogous to equation (39), tortuosity is expressed as

$$\tau_a = \frac{\theta_a^{7/3}}{n^2} . \tag{44}$$

And, in an alternative Millington-Quirk model (MQ2) evaluated by Jin and Jury (1996), tortuosity is expressed as

$$\tau_a = \frac{\theta_a}{n^{2/3}} . \tag{45}$$

Note that as θ_a approaches n (e.g. as the porous medium becomes drier), τ_a approaches $n^{1/3}$ for both formulations (44) and (45).

An air-phase tortuosity model was developed by Lahvis et al. (1999) by calibrating a transport model to steady-state gas concentration data obtained from seven column experiments using silt and fine sand sediments. In this model, air phase tortuosity is dependent only on the volumetric water content:

$$\tau_a = 0.765 - 2.02\ \theta_w. \tag{46}$$

Comparison of these models for alluvium with an effective porosity of 0.37 and tortuosity as defined in equation (38) is shown in Figure 18. Due to the similarity of the Lahvis et al. (1999) model to the MQ2 model over a wide range of volumetric water content, it will not be considered further.

The Penman and the two Millington-Quirk models were compared by Jin and Jury (1996) with measured D_{eff}/D_{bulk} ratios from six studies that included a total of approximately 50 measurements on predominantly agricultural soils. While this ratio corresponds to the definition of tortuosity given in equation (38), it is useful in comparing the predictions of the various models. Over the range of air phase porosity investigated (0.05 to 0.5), the Penman model tended to overestimate tortuosity, while the MQ1 model in equation (44) underestimated tortuosity. Of the three models, the MQ2 model given by (45) provided the best fit to the measured tortuosities.

A comparison of the Penman and Millington-Quirk models for a material with an effective porosity of 0.37 is shown in Figures 18 and 19. Note that in both these figures, the points are merely points of calculation, and do not represent data. The values produced by the Penman and Millington-Quirk models converge for dry and wet conditions but diverge at intermediate values of air porosity. Given its median behavior as seen in Figures 18 and 19, the alternative Millington-Quirk model (MQ2, equation (45)) is used in the Clive DU PA model.

Tortuosity is implemented in the GoldSim model as a multiplier to the diffusive length, which is defined for each Cell Pathway element using the common method of setting it equal to 1/2 the cell length that is parallel to flow. In this case, that is the vertical dimension.

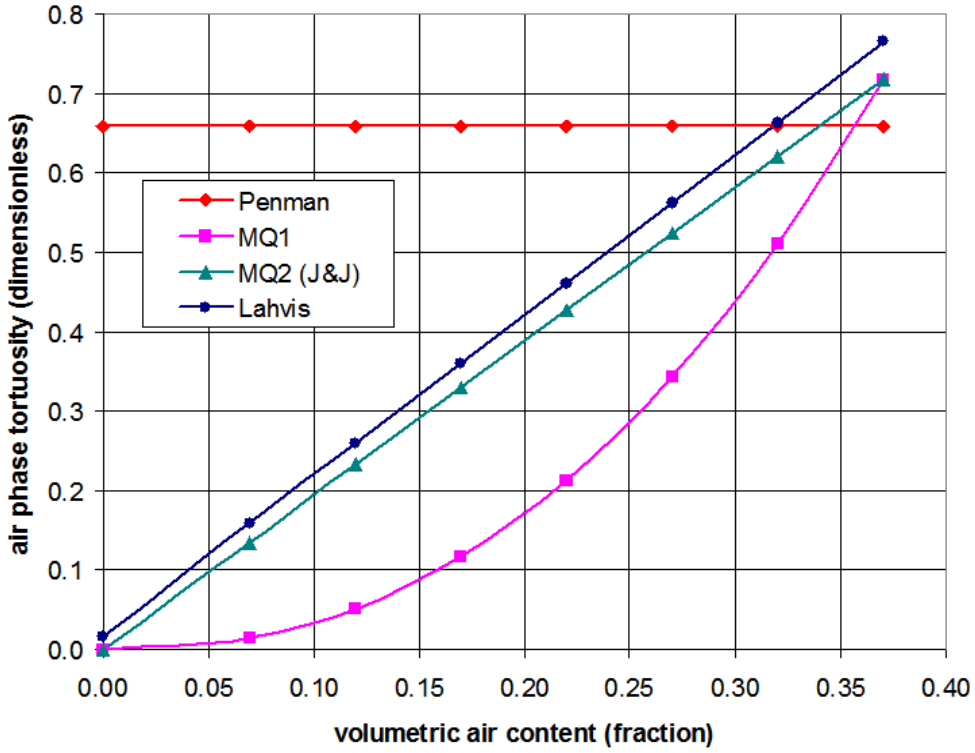

Figure 18. Comparison of air-phase tortuosity models by Penman (equation (43)), Millington and Quirk (MQ1, equation (44)), Millington and Quirk as modified by Jin and Jury (1996) (MQ2, equation (45)), and Lahvis et al. (1999) (equation (46)).

9.3 Air/water partitioning: Henry's Law

Most volatile solutes exist to varying degrees in both air and water. In the absence of other processes, a solute will partition between air and water phases in a given proportion (for a given temperature), following Henry's Law. The ratio of the concentration of a chemical in water to its concentration in air in known as its Henry's Law constant, which can have many functional forms. In the Clive DU PA Model, only one radionuclide has a gaseous phase: radon. Sander (1999, Table 7, p.13) provides a Henry's Law constant for radon of 9.3×10^{-3} mol/L·atm, defined using a form of Henry's Law that relates the partial pressure of the solute in the gas above the water to the concentration of the water:

$$K_{H,cp} = \frac{c}{p} \tag{47}$$

where

$K_{H,cp}$ is the Henry's Law constant relating c to p, in units of mol/L·atm
c is the concentration of the solute, in mol/L, and
p is the partial pressure of the solute in the gas phase, in atm.

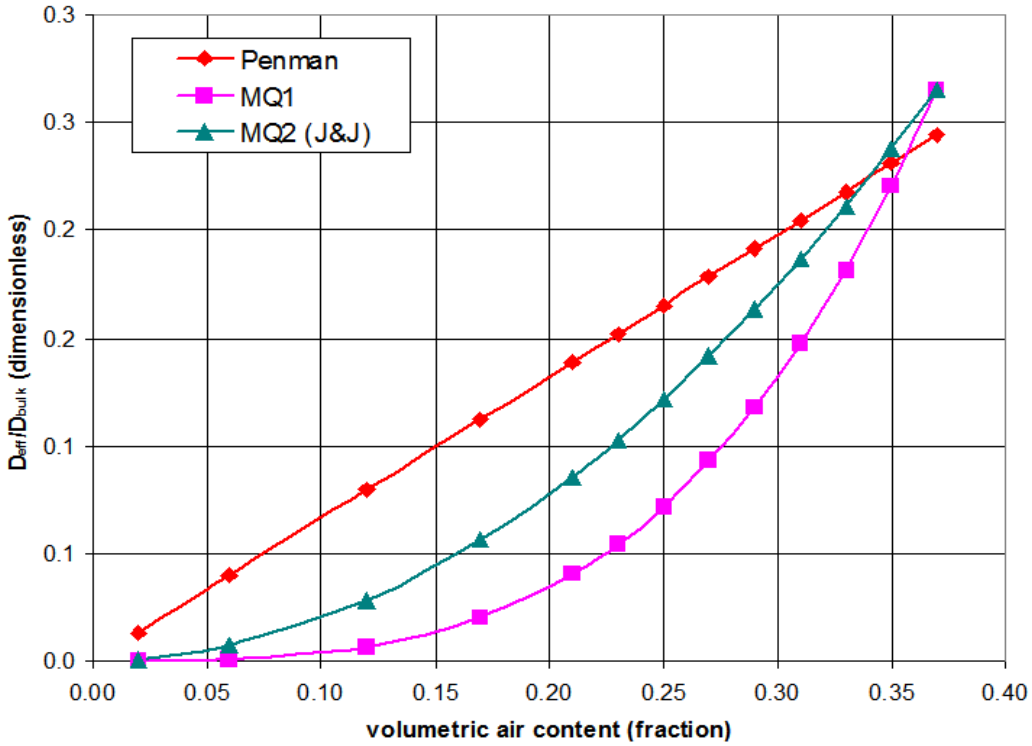

Figure 19. Comparison of effective to bulk diffusivity ratios with air phase porosity for air phase tortuosity models.

This Henry's Law constant must be converted to the dimensionless form—a ratio of the concentration in water to that in gas (air):

$$K_H = \frac{C_{(water)}}{C_{(air)}} \tag{48}$$

This conversion is done using the following equation:

$$K_H = \frac{1}{K_{H,cp} R T_{soil}} \tag{49}$$

where

R is the ideal gas constant, and
T_{soil} is the soil temperature.

The gas constant R is conveniently provided as a defined constant in GoldSim. The soil temperature at the Clive facility is estimated from the Clive Test Cell data provided by Energy*Solutions* in the spreadsheet "Temp and Dose Data 9-19-01 to 1-15-09.xls", with a normal distribution with a mean of 12°C and a standard deviation of 1 °C.

This dimensionless Henry's Law constant K_H for radon is an attribute of the fluid material Air defined in the Clive DU PA Model. The value of K_H for radon is therefore 4.5, meaning that the noble gas strongly favors dissolution in water.

9.4 Transport of Radon

The Clive DU PA Model is dominated by a single waste form: depleted uranium. This material predominantly consists of ^{238}U. This uranium isotope is a parent of ^{222}Rn, its rate of production controlled by the decay rate of the ^{238}U. Using a basic representation of fate and transport, radon emanation is accounted for, as is Henry's Law partitioning into water, and the gas is allowed to diffuse in pore air using GoldSim's internal diffusion processes, as corrected for unsaturated media and for numerical dispersion. Radon emanation and diffusion are discussed below.

9.4.1 Radon Emanation (Escape/Production Ratio)

The fraction of ^{222}Rn produced by decay of radium-226 (^{226}Ra) that is released from the solid matrix is known as the escape-to-production (E/P) ratio, as well as the emanation coefficient, the emanation factor, or emanating power (Nielson and Sandquist, 2011). When ^{226}Ra decays, a small fraction of the decay energy, 0.1 MeV, is carried by the recoiling ^{222}Rn atom. This is sufficient energy for the recoiling atom to travel about 45 nm in a mineral matrix, 0.1 μm in water, and about 63 μm in air. Recoiling atoms with just sufficient energy to stop in the air or water filled pore space will be released from the matrix and become available for transport. If there is too little energy available, the atom will remain trapped in the solid matrix. If there is too much energy, the atom will cross the pore space and be embedded in the solid matrix of a nearby grain. The E/P ratio describes that fraction of ^{222}Rn that stops in the air or water-filled pore space and is free to diffuse. The E/P ratio can physically vary from a minimum of 0 to a maximum of 1.

Predicting the E/P ratio for a material is difficult as numerous factors have been identified that affect it: The E/P ratio is inversely related to grain size. The closer decaying atoms are to the surface of a grain, the more likely they will be released to the pore space. The adsorption or coprecipitation of ^{226}Ra on surficial coatings increases emanation, as will cracks, fissures, or pitting of grains. In contrast, the E/P ratio is directly related to pore size. As the pore size increases, it is more likely that recoiling atoms will stop in the pore space and emanation increases. The presence of water in the pore space increases emanation, because the reduced particle range in water increases the likelihood that the recoiling atom will stop in the pore space. Predicting the E/P ratio of a material is particularly difficult because it requires detailed knowledge of the microscopic physical structure of the material, microscopic distribution of ^{226}Ra in the material, and water content.

The E/P ratios for different types of common geologic materials have been reported. From geometrical considerations, the maximum emanation expected from a thick slab source is 0.5 and from a thin film, 1.0. The maximum E/P ratio of natural materials will lie somewhere between these two extremes. The maximum value reported for common materials is approximately 0.7 to 0.8. Reported E/P ratios for soils and rocks range from 0.02 to 0.7 (UNSCEAR 2000; NCRP 1988). The emanation factor of a single material may vary over a substantial portion of this range depending on the water content. Rock and uncrushed ores usually have lower emanation factors ranging from 0.02 to 0.26 (Nazaroff 1992). Concrete emanation factors may range from 0 to 0.3 (Rogers et al. 1994; Cozmuta et al. 2003).

Nielson and Sandquist (2011, Table 1, p. 11) discuss radon modeling at length, and have assembled information about E/P ratios in uranium ores (in Table 1 of that document), which are reasonable analogs for uranium oxides that are the subject of this PA. Following the principles outlined in the *Fitting Probability Distributions* white paper, a beta distribution is chosen to represent the E/P ratio, with a mean of 0.290, with a standard deviation of 0.156.

9.4.2 Radon diffusion

The transport of the radioactive noble gas radon presents special modeling challenges. The diffusion of gas phase constituents follows concentration gradients, and these vary along the diffusive path. These concentrations are subject to other transport processes, notably partitioning into water (according to the Henry's Law constant) and encountering sinks like the atmosphere. In the modeling of radioactive constituents, most radionuclides have relatively long half-lives, and the concentration gradients are not much affected by decay and ingrowth. Radon isotopes, however, have short half-lives relative to the rate of diffusive transport processes, can move quickly in pore air, and decay to a chain of radionuclides that can be significant in terms of dose and risk. In the Clive DU PA Model, the radon isotope of interest is ^{222}Rn, with a half-life of about 3.8 days. With this short half-life, ^{222}Rn decays away quickly enough that the decay alone can produce strong concentration gradients, causing additional challenges in numerical simulation.

Chemical engineers are faced with similar issues in process plants, where chemicals in a process that moves through the plant are simultaneously undergoing chemical transformation to other substances. The quantification of this effect is called the Damköhler number. The value can be expressed in a number of different ways for different applications, and in the case of this model, it is the ratio of the decay rate to the diffusive mass transport rate. For ^{222}Rn, with its high rate of decay, the Damköhler number is also high, indicating that diffusive transport will be overpredicted in a coarsely-discretized model such as the Clive DU PA Model.

Approaches to correcting for this overprediction include calibration to analytical solutions for radon diffusive transport and refining the discretization of the modeling grid. If the contaminant transport modeled column is of one or two layers of uniform materials, analytical solutions are possible, such as those presented in the Nuclear Regulatory Commission's Regulatory Guide on the estimation of radon attenuation in earthen covers for uranium mill tailings piles (NRC 1989b).

9.4.3 Calibration of Air Diffusion to Counteract Numerical Dispersion

In the Clive DU PA Model, where wastes and other materials with a variety of porous medium properties can be intermixed, calibration to analytical solutions is prohibitively difficult. The only way to refine the solution is by refining the grid, which is the approach that is taken in the model. This refinement reduces numerical dispersion, providing a realistic simulation of the diffusion process. To refine the top slope and side slop columns, which integrate all the contaminant transport processes, would introduce an unreasonable computational burden, since most of the processes would not appreciably benefit from the finer discretization. By taking advantage of a clever side calculation, the model can benefit from the increased accuracy of the finer discretization, without significant computational effort.

Within the GoldSim container for the Class A South Top Slope contaminant transport calculations, an additional container is added, with a switch for enabling and disabling its calculations. This container is devoted to determining the appropriate measure by which the radon diffusivity of 0.11 cm^2/s should be reduced in order to exactly counter the effects of numerical dispersion. The calculation consists of two columns: one coarsely- and one finely-discretized. The coarse discretization matches that of the main Top Slop column, with GoldSim Cell pathway elements representing layers in the cover of about 15 cm (6 in) thickness, and layers in the waste about 50 cm (20 in) thick. Each of the Cells is populated with air, water, porous media, and initial inventory just as is the main column, but the only processes represented include retardation, solubility, and air diffusion. This protects the coarse column from all the confounding factors of water advection and diffusion, biotic processes, etc.

The fine column is built the same way, but with 15 times as many Cells. That is, the cover cells in the fine column are about 1 cm thick, and those in the waste are about 3 cm. This fine column has significantly less numerical dispersion for the air diffusion calculations, and is used for calibration of the coarse column. The calibrated diffusion coefficients for radon in the coarse column, then, are also applied to the main Top Slope and Side Slope columns, thereby counteracting the effects of numerical dispersion there as well.

Both the coarse and fine columns are populated with porous materials that exactly match those in the Top Slope column. These reside in three distinct zones. From the bottom up, these zones are: 1) the waste zone, where radioactive wastes are disposed, and are of similar material properties as far as air diffusion is concerned, 2) the radon barrier clay layers, which consist of tightly compacted clays overlying the wastes, and 3) the upper cover materials, which are uncompacted fill materials. The radon fluxes (mass flow per area, with dimensions of M/L^2-T and units of g/m^2-s or pCi/m^2-s) are recorded at the top of each of these three zones in both the coarse and fine columns. With less numerical dispersion, the finer column always has a lower rate of diffusion out the top of the zone.

If the coarse column's diffusion coefficient for radon is adjusted downward, it can be forced to match the finer column, producing a more accurate flux. This correction is performed sequentially, from the bottom up, and a different correction factor is applied for each material within the three zones. This results in one radon diffusion correction factor for the waste zone, one for the clays, and one for the upper cover layers. The correction factor for wastes is applied to the waste layers in the Top Slope and Side Slope contaminant transport columns. Likewise, the correction factors for the clay layers is applied to the radon barrier clay and liner clay layers in the Top Slope and Side Slope columns, and the correction factors for the upper cover layers is applied to both columns as well.

This radon calibration need be done only once, unless the layer geometries and/or material properties change significantly. Fortunately, performing the calibration in deterministic mode is sufficient, as it is robust and holds quite well even using stochastic inputs in probabilistic mode. Once the calibration has been completed, the radon calibration container may be disabled, so that it does not impose further computational burden on the model.

10.0 References

Abramowitz, Milton, and Irene A. Stegun, 1970. *Handbook of Mathematical Functions with Formulas, Graphs, and Mathematical Tables*. National Bureau of Standards, Applied Mathematics Series 55, ninth printing. November, 1970.

Albright, W.H., G.W. Gee, G.V. Wilson, and M.J. Fayer. 2002. *Alternative Cover Assessment Project Phase I Report.* Desert Research Institute Publication No. 41183. Reno, NV.

Bingham Environmental, 1991. *Hydrogeologic Report Envirocare Waste Disposal Facility South Clive, Utah*. Final version October 9, 1991.

Bingham Environmental, 1994. *Hydrogeologic Report Mixed Waste Disposal Area Envirocare Waste Disposal Facility South, Clive, Utah*. Final version November 18, 1994.

Buckingham, E. 1907. *Studies on the Movement of Soil Moisture*. Bulletin 38. U.S. Dept. of Agriculture Bureau of Soils. Washington, D.C.

Clennell, M.B. 1997. *Tortuosity: a guide through the maze*. in Developments in Petrophysics, Lovell, M.A. and P.K. Harvey (eds). Geological Society Special Publication No. 122, pp. 299-344.

Conca, J.L., and J.V. Wright. 1992. Flow and Diffusion of Unsaturated Gravel, Soils and Whole Rock, *Applied Hydrogeology*, International Association of Hydrogeologists, Vol. 1, 1992, pp. 5-24.

Cozmuta, I., E. R. van der Graaf, and R. J. de Meijer, 2003. Moisture Dependence of Radon Transport in Concrete: Measurements and Modeling. *Health Physics* 85(4): 438 – 456.

Domenico, P.A. and F.W. Schwartz. 1990. *Physical and Chemical Hydrogeology*. John Wiley & Sons, New York, NY.

EnergySolutions, 2009. *Class A South Cover Designs. Drawing 07021 V7*, Clive, Utah.

Envirocare, 2005. *Cover Test Cell Data Report Addendum: Justification to Change EZD from 18-inches to 24-inches*. Attachment to letter dated October 13, 2005 from Daniel B. Shrum, Director of Safety and Compliance, Envirocare of Utah, LLC, to Dane L. Finefrock, Executive Secretary, Division of Radiation Control.

Fayer, M.J., 2000. *UNSAT-H Version 3.0: Unsaturated Soil Water and Heat Flow Model, Theory, User Manual, and Examples*. PNNL-13249. Pacific Northwest National Laboratory, Richland, Washington. June, 2000.

Freeze, R.A and J.A. Cherry. 1979. *Groundwater*. Prentice-Hall, Inc., Englewood Cliffs, NJ.

GTG (GoldSim Technology Group), 2011. *User's Guide: GoldSim Contaminant Transport Module*, GoldSim Technology Group, Issaquah, WA, December 2010

Hillel, D. 1980. *Fundamentals of Soil Physics*. Academic Press Inc. San Francisco, CA.

Jin, Y., and W.A. Jury. 1996. *Characterizing the Dependence of Gas Diffusion Coefficient on Soil Properties*, Soil Science Society of America Journal, Vol. 60, pp. 66-71.

Jury, W.A. and R. Horton. 2004. *Soil Physics.* 6th ed. John Wiley and Sons Inc. New Jersey.

Khire, M.V., C.H. Benson, and P.J. Bosscher. 1997. Water balance modeling of earthen final covers. *J. Geotechnical and Geoenvironmental Engineering* . Vol. 23, No. 8.

Koorevaar, P., G. Menelik, and C. Dirksen. 1983. *Elements of Soil Physics*. Elsevier. New York, NY.

Lahvis, M.A., A.L. Baehr, and R.J. Baker. 1999. *Quantification of Aerobic Biodegradation and Volatilization Rates of Gasoline Hydrocarbons Near the Water Table Under Natural Attenuation Conditions*. Water Resour. Res. v. 27, 753-765.

Marsily, G. de. 1986. *Quantitative Hydrogeology*. Academic Press Inc. San Diego, CA.

Meyer, P.D., M.L. Rockhold, W.E. Nichols, and G.W. Gee. 1996. *Hydrologic evaluation methodology for estimating water movement through the unsaturated zone at commercial low-level radioactive waste disposal sites.* NUREG/CR-6346. U.S. Nuclear Regulatory Commission. Washington, D.C.

Millington, R.J., and J.P. Quirk. 1961. "Permeability of porous solids." Trans. Faraday Society (57) pp. 1200-1207

Mualem, Yechezkel, 1976. *A New Model for Predicting the Hydraulic Conductivity of Unsaturated Porous Media*. Water Resources Research, Vol. 12, No. 3, pp. 513-522. June, 1976.

Nazaroff, W. W., 1992. Radon Transport from Soil to Air. Rev. of Geophysics 30(2): 137 – 162.

NCRP (National Council on Radiation Protection and Measurements). 1988. Measurements of Radon and Radon Daughters in Air. NCRP Report No. 97, NCRP Bethesda, Maryland, November 1988.

NRC (U.S. Nuclear Regulatory Commission). 1989b. *Calculation of Radon Flux Attenuation by Earthen Uranium Mill Tailings Covers, Regulatory Guide 3.64*, Nuclear Regulatory Commission, June 1989.

Nielson, K.K., and G.M. Sandquist. 2011. *Radon Emanation from Disposal of Depleted Uranium at Clive, Utah*. Report for Energy*Solutions* by Applied Science Professionals, LLC. February 2011.

Penman, H.L. 1940. "Gas and vapor movements in the soil. I. The diffusion of vapors through porous solids." Journal of Agricultural Science (30) pp. 437-462

Rogers, V.C., and K.K. Nielson. 1991. Correlations for Predicting Air Permeabilities and Rn-222 Diffusion Coefficients of Soils, Health Physics (61) 2

Rogers, V.C., K. K. Nielson, M. A. Lehto, and R. B. Holt, 1994. Radon Generation and Transport Through Concrete Foundations. EPA/600/SR-94/175, U. S. Environmental Protection Agency, Research Triangle Park, North Carolina, November 1994.

Sander. 1999. Compilation of Henry's Law Constants for Inorganic and Organic Species of Potential Importance in Environmental Chemistry, version 3, 8 Apr 1999 http://www.mpch-mainz.mpg.de/~sander/res/henry.html

Schroeder, P.R., Aziz, N.M., Lloyd, C.M., and P.A. Zappi, 1994. *The Hydrologic Evaluation of Landfill Performance (HELP) Model: User's Guide for Version 3*, EPA/600/R-94/168A; US EPA Office of Research and Development, Washington, D.C.

SWCA, 2011, *Field Sampling of Biotic Turbation of Soils at the Clive Site, Tooele County, Utah*, SWCA Environmental Consultants, Salt Lake City, Utah, January 2011.

UNSCEAR (United Nations Scientific Committee on the Effects of Atomic Radiation). 2000. UNSCEAR Report to the General Assembly – Sources and Effects of Ionizing Radiation.

USDA (United States Department of Agriculture) 2011. Web Soil Survey. US Department of Agriculture, National Resources Conservation Service. 2011. Retrieved from URL http://websoilsurvey.nrcs.usda.gov/.

Ward, A.L., M.D. White, E.J. Freeman, and Z.F. Zhang. 2005. STOMP: *Subsurface transport over multiple phases. Version 1.0. Addendum: Sparse vegetation evapotranspiration model for the water-air-energy operational mode.* PNNL-15465. Pacific Northwest National Laboratory, Richland, WA.

Whetstone Associates, Inc., 2000, *Revised Envirocare of Utah Western LARW Cell Infiltration and Transport Modeling.* July 19, 2000.

Whetstone Associates, Inc., 2007. *EnergySolutions Class A South Cell Infiltration and Transport Modeling*. December 7, 2007.

Wolfsberg, A. and P. Stauffer. 2003. *Vadose Zone Fluid and Solute Flux: Advection and Diffusion at the Area 5 Radioactive Waste Management Site*. LA-UR-03-4819, Los Alamos National Laboratory, Los Alamos, New Mexico.

Appendix

Soil Moisture Data for Units 3 and 4

The data for soil moisture characteristics in Unit 3, a silty sand, and in Unit 4, a silty clay, are reproduced in the following tables, and are based on testing performed by Colorado State University (Bingham Environmental 1991, Appendix B, pages B-20 and B-26). Cores GW18-B4 and GW79A-B5 are from Unit 3, and cores GW19A-B1 and GW17A-B2 are from Unit 4. Bulk density is defined in the units of g/cm^3. Conductivity data have units of cm/s.

	GW18-B4		GW19A-B1		GW17A-B5		GW17A-B2	
	WATER CONTENT	MATRIC PRESSURE (cm)	WATER CONTENT	MATRIC PRESSURE (cm)	WATER CONTENT	MATRIC PRESSURE (cm)	WATER CONTENT	MATRIC PRESSURE (cm)
DRYING CYCLE	0.409	0	0.442	0	0.377	0	0.505	0
	0.409	6	0.438	383	0.376	19	0.505	49
	0.404	24	0.426	468	0.319	60	0.485	455
	0.362	94	0.405	683	0.207	274	0.466	954
	0.321	131	0.370	1074	0.188	569	0.453	1947
	0.262	171	0.344	2029			0.429	2563
	0.213	230	0.337	3025			0.397	4815
	0.180	349	0.316	4921				
	0.144	664						
	0.132	828						
WETTING CYCLE	0.117	932	0.316	4211	0.1279	946	0.395	4030
	0.119	852	0.317	3961	0.128	807	0.396	3537
	0.122	817	0.317	3736	0.128	578	0.399	3092
	0.126	683	0.322	3465	0.130	403	0.403	2545
	0.129	633	0.323	3265	0.134	282	0.407	2045
	0.135	491	0.327	3010	0.148	204	0.410	1524
	0.142	417	0.332	2774	0.186	88	0.413	1005
	0.156	314	0.335	2540	0.254	53	0.417	504
	0.171	262	0.343	2284	0.307	49	0.422	211
	0.180	221	0.345	2054	0.316	34	0.426	60
	0.220	110	0.352	1804				
	0.302	36	0.357	1534				
	0.327	9	0.365	1300				
			0.369	1079				
			0.373	845				
			0.383	625				
			0.398	391				
			0.397	300				
			0.432	0				
BULK DENSITY	1.567		1.397		1.673		1.326	
POROSITY	0.409		0.473		0.320		0.505	
WETTING CYCLE FIT PARAMETERS								
θ_s	0.380		0.432		0.345		0.429	
θ_s	0.0		0.0		0.130		0.172	
α	0.05222		0.00295		0.0177		0.0012	
n	1.3068		1.1202		3.6477		1.1000	
m	0.2347		0.1073		0.7259		0.0909	

	GW18-B4		GW19A-B1		GW17A-B5	
	WATER CONTENT	D(θ) (cm^2/s)	WATER CONTENT	D(θ) (cm^2/s)	WATER CONTENT	D(θ) (cm^2/s)
DIFFUSIVITY DATA	0.380	0.005559	0.430	0.004502	0.345	0.005559
	0.360	0.010385	0.420	0.004024	0.340	0.012307
	0.340	0.008981	0.400	0.003327	0.320	0.008794
	0.320	0.008246	0.380	0.002838	0.300	0.007767
	0.300	0.007759	0.360	0.002471	0.280	0.007184
	0.280	0.007401	0.340	0.002184	0.260	0.006785
	0.260	0.007119	0.320	0.001952	0.240	0.006485
	0.240	0.006889	0.315	0.001900	0.220	0.006247
	0.220	0.006696	0.312	0.001870	0.200	0.006051
	0.200	0.006529	0.262	0.001468	0.180	0.005885
	0.180	0.006383	0.212	0.001186	0.160	0.005742
	0.160	0.006254	0.162	0.000974	0.140	0.005616
	0.140	0.006138	0.112	0.000809	0.135	0.005586
	0.120	0.006034			0.132	0.005569
	0.100	0.005938			0.1308	0.005563
	0.080	0.005850			0.1305	0.005561
	0.060	0.005770				
	0.040	0.005695				
	0.020	0.005625				
	0.010	0.005591				
CONDUCTIVITY DATA	0.380	3.38E-5	0.430	1.89E-7	0.345	5.59E-5
	0.360	3.28E-5	0.420	1.33E-7	0.340	9.60E-6
	0.340	2.42E-5	0.400	6.74E-8	0.320	1.72E-5
	0.320	1.74E-5	0.380	3.41E-8	0.300	1.76E-5
	0.300	1.22E-5	0.360	1.71E-8	0.280	1.55E-5
	0.280	8.39E-6	0.340	8.38E-9	0.260	1.25E-5
	0.260	5.59E-6	0.320	4.01E-9	0.240	9.16E-6
	0.240	3.61E-6	0.315	3.32E-9	0.220	6.09E-6
	0.220	2.25E-6	0.312	2.96E-9	0.200	3.53E-6
	0.200	1.34E-6	0.262	3.84E-10	0.180	1.65E-6
	0.180	7.56E-7	0.212	3.49E-10	0.160	5.01E-7
	0.160	4.00E-7	0.162	1.79E-12	0.140	3.62E-8
	0.140	1.95E-7	0.112	3.28E-14	0.135	6.65E-9
	0.120	8.54E-8			0.132	6.45E-10
	0.100	3.22E-8			0.1308	4.73E-11
	0.080	9.83E-9			0.1305	9.10E-12
	0.060	2.14E-9				
	0.040	2.50E-10				
	0.020	6.44E-12				
	0.010	1.67E-13				
FIT PARAMETER Ks	4.4E-3		2.00E-4		2.00E-4	